AD-A130 877 FURTHER RESULTS ON THE PREDICTIONS OF COLLAPSE PRESSURE OF A RING STIFFEN.. (U) NAVAL SURFACE WEAPONS CENTER SILVER SPRING MD M MOUSSOUROS SEP 82 NSWC/TR-82-172 1/1

UNCLASSIFIED SBI-AD-F500 168 F/G 20/11 NL

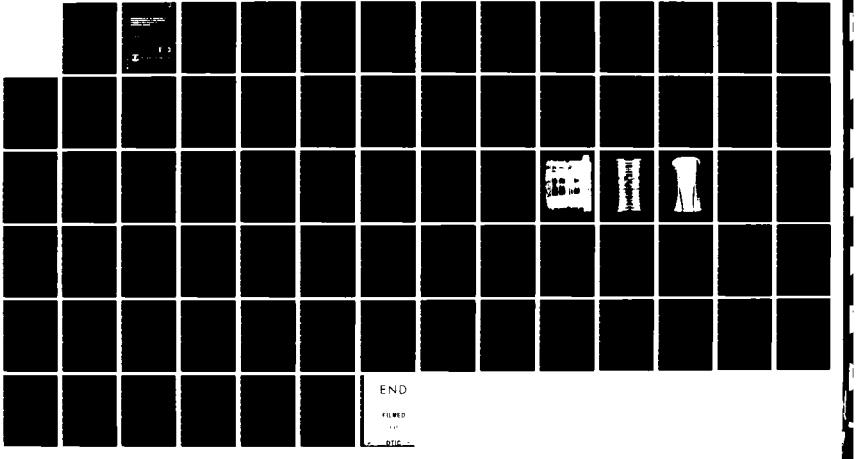

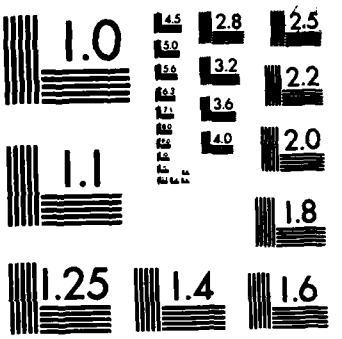

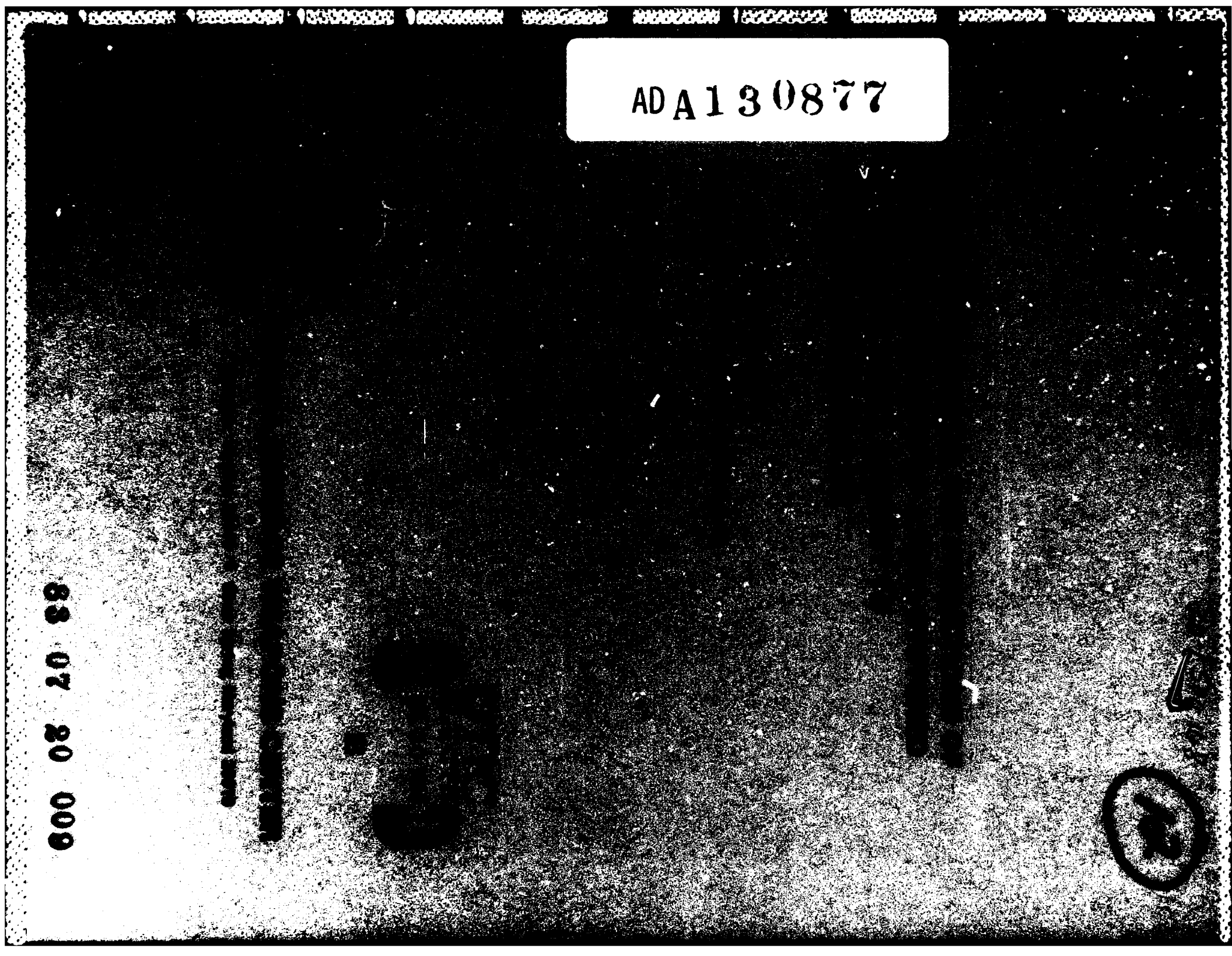

UNCLASSIFIED

SECURITY CLASSIFICATION OF THIS PAGE (When Data Entered)

REPORT DOCUMENTATION PAGE		READ INSTRUCTIONS BEFORE COMPLETING FORM
1. REPORT NUMBER NSWC TR 82-172	2. GOVT ACCESSION NO. AD-A130 877	3. RECIPIENT'S CATALOG NUMBER
4. TITLE (and Subtitle) FURTHER RESULTS ON THE PREDICTIONS OF COLLAPSE PRESSURE OF A RING STIFFENED CYLINDRICAL SHELL SUBJECT TO HYDROSTATIC PRESSURE		5. TYPE OF REPORT & PERIOD COVERED Documentation 6. PERFORMING ORG. REPORT NUMBER
7. AUTHOR(s) Minos Moussouros		8. CONTRACT OR GRANT NUMBER(s)
9. PERFORMING ORGANIZATION NAME AND ADDRESS Naval Surface Weapons Center (Code R14) White Oak, Silver Spring, MD 20910		10. PROGRAM ELEMENT, PROJECT, TASK AREA & WORK UNIT NUMBERS 63610N; 50-199-600-0-2R19BB429
11. CONTROLLING OFFICE NAME AND ADDRESS		12. REPORT DATE September 1982 13. NUMBER OF PAGES 68
14. MONITORING AGENCY NAME & ADDRESS(if different from Controlling Office)		15. SECURITY CLASS. (of this report) UNCLASSIFIED 15a. DECLASSIFICATION/DOWNGRADING SCHEDULE

16. DISTRIBUTION STATEMENT (of this Report)
Approved for public release; distribution unlimited.

17. DISTRIBUTION STATEMENT (of the abstract entered in Block 20, if different from Report)

18. SUPPLEMENTARY NOTES

19. KEY WORDS (Continue on reverse side if necessary and identify by block number)
Static Collapse

20. ABSTRACT (Continue on reverse side if necessary and identify by block number)
This study reassesses the critical static buckling load of a ring reinforced circular shell as obtained by the nonlinear finite element code STAGS for a variety of boundary conditions and compares it more conclusively with values from other sources. The influence of a rectangular opening on the elastic buckling strength is also addressed. A modeling procedure is being recommended for such problems.

DD FORM 1 JAN 73 1473 EDITION OF 1 NOV 65 IS OBSOLETE
S/N 0102-LF-014-6601

UNCLASSIFIED

SECURITY CLASSIFICATION OF THIS PAGE (When Data Entered)

FOREWORD

This study reassesses the critical static buckling load of a ring reinforced circular shell as obtained by the nonlinear finite element code STAGS for a variety of boundary conditions and compares it more conclusively with values from other sources. The influence of a rectangular opening on the elastic buckling strength is also addressed. A modeling procedure is being recommended for such problems.

Approved by:

T. W. Austin for

J. F. PROCTOR, Head
Energetic Materials Division

Accession For	
NTIS GRA&I	☑
DTIC TAB	☐
Unannounced	☐
Justification	
By	
Distribution/	
Availability Codes	
Dist	Avail and/or Special
A	

CONTENTS

CONTENTS (Cont.)

ILLUSTRATIONS

ILLUSTRATIONS (Cont.)

ILLUSTRATIONS (Cont.)

ILLUSTRATIONS (Cont.)

TABLES

CHAPTER 1

INTRODUCTION

The ultimate objective of this work is to obtain accurate predictions of the effect of structural damage on the collapse strength of submarine pressure hulls. Therefore, it is necessary that a procedure be established for determining the critical static buckling load of typical hull structures with and without pre-damage.

Reference 1 used the finite element method to address itself, albeit in a narrow way, to the question of critical static collapse pressure. However, several advanced issues were not treated there. These relate to the effect of circumferential boundary conditions, the use of half and quarter models, the effect of mesh size on eigenvalues, plate element types, the effect of a hole, and finally, the effect on the result of deviations from a purely cylindrical geometry. It is the intention of this report to address these topics, particularly in the context of a finite element buckling analysis which presents considerable practical difficulties.

---

[1] Moussouros, M., Comparisons of Static Collapse Predictions of a Ring Stiffened Cylindrical Shell Subject to Hydrostatic Pressure, NSWC TR 81-325, 3 Mar 1982.

CHAPTER 2

BACKGROUND TO CRITICAL LOAD ANALYSIS

In the following paragraphs we briefly discuss the phenomenon of buckling of a structure.

When a structure is subjected to compressive external loads there always exists a critical load above which deformations and strains increase so drastically that the load carrying capacity of the structure is impaired. This notion of the critical load is very useful to damage prediction.

To describe this instability phenomenon, one may form the potential energy functional of the discrete equivalent system in terms of the generalized coordinates q_i (displacements) *and a loading factor* λ *in the form*

$$V(q_i, \lambda) = U(q_i) - \lambda f(q_i)$$

where $U(q_i)$ is the strain energy of the structure and $f(q_i)$ is a function of the deformations (generalized coordinates) and $\lambda f(q_i)$ is a term representing the work done on the structure. The changes of such a functional are excellent indicators of the behavior of the system. Moreover, the separate contributions to strain energy may offer further insight as to which terms dominate as the point of instability is approached.

Geometrically, the maxima and minima of the curve relating q_i and λ are limit points. There the stability of an equilibrium path changes and the total potential energy has an inflexion. In general, there may be several equilibrium paths, with intersections referred to as "bifurcation points." For example, in the case of the Euler column subject to an axial compressive load, the primary path and the secondary path cross at a bifurcation point known as the Euler

buckling load. Bifurcation points may be further classified as either asymmetric, stable-symmetric, or unstable-symmetric, depending on whether the potential energy has an inflexion, a minimum (second variation positive), or a maximum, (second variation negative). With this background we proceed to the modeling process.

CHAPTER 3

STRUCTURAL MODELING

We start by describing the steps involved in an analysis by the finite element method.

(1) Develop a model of the real structure, say an internally stiffened cylinder, by subdividing it into elements (Figure 1) of various shapes. In attempting to model the expected behavior of the structure, it should be noted that different element types and their arrangement may alter the results drastically. A way to include imperfections must be devised. This may be a more important factor in buckling computations than in many other types of structural analysis. In deciding how much of the cylindrical structure to include in the model, we note that we could consider an arbitrary number of bays away from the ends, provided they are equidistant. We may impose continuity conditions at arbitrary cuts for symmetrical structures with symmetrical loading. In the present instance, it appears reasonable to use a minimum of three bays.

(2) Obtain required "inputs" including material properties, plate thicknesses, properties of members, etc.

(3) Simulate, as exactly as possible, the boundary conditions, whether they are of the stress or displacement type. Furthermore, using a half or a quarter model of the structure, the computer requirements for the analysis can be reduced considerably. This action, however, requires additional boundary conditions at the interfaces, and these may, themselves, create difficulties which must be considered in buckling problems.

(4) Impose the external loading known as the baseload. This can then be magnified by a loading factor. Applying the external, longitudinal,

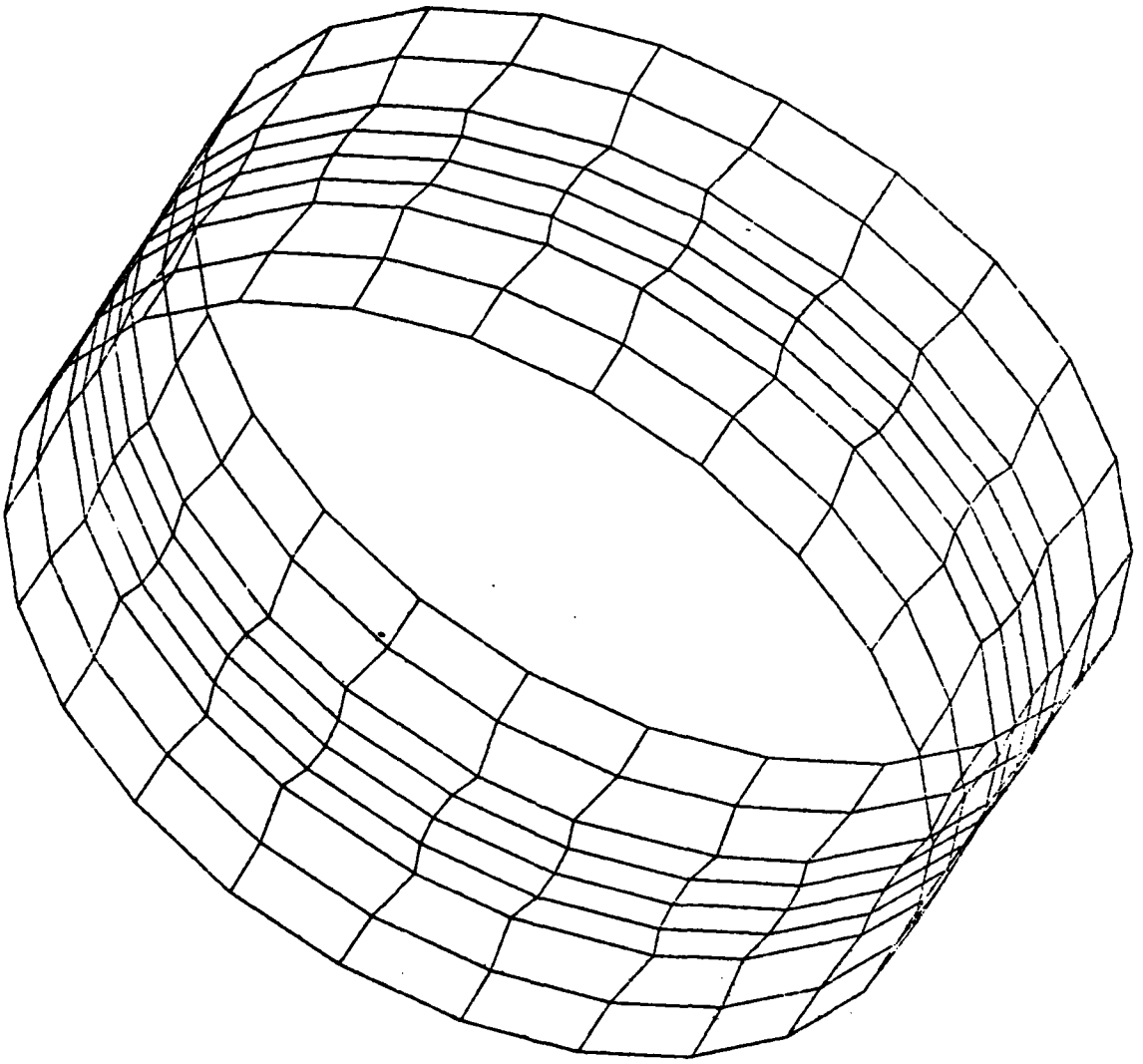

FIGURE 1. MODE 1 FOR CASE 1, FULL MODEL, ΔP_{cr} = 263.38 LB/IN^2

compressive forces can be achieved in a variety of ways. One may include heavy end plates which model the end closures and, simultaneously, attempt to avoid their buckling and then enforce the pressure load. This method would result in heavy local bending at the junctions, possibly affecting the buckling mode. Another method, the one employed in this report, is to introduce the end pressure as a uniform axial line load (Reference 2).

(5) Reconsider items (1) - (4) when the shell contains a hole.

---

[2]Moussouros, M., Comparisons of Static Collapse Predictions of a Ring Stiffened Cylindrical Shell Subject to Hydrostatic Pressure.

CHAPTER 4

APPLICATION

In Reference 3, a portion of a WW II submarine was analyzed using the STAGS[4] general shell finite element program. The bifurcation (linear stress state) option, employing the full length of three frame spaces, but only a semicircular portion of the modeled cylinder was used. At the resulting axial cuts $\theta = 0$ and $\theta = \pi$ (Figure 2) symmetry conditions were employed. It was later realized that such an analysis might not yield the lowest critical pressure.

It will shortly be evident that mesh size, choice of plate element, and deviations from a perfect cylindrical geometry may be significant. The choice of boundary conditions, such as the ones imposed to reduce the dimensionality of the analysis, may also affect the results. These points were not addressed in Reference 5. Therefore, in order to be more comprehensive, irrespective of the presence or absence of predamage, this study investigates:

(1) The effect of boundary conditions used to reduce dimensionality of the problem;

(2) The effect of mesh refinement on computed eigenvalues;

---

[3]Moussouros, M., Comparisons of Static Collapse Predictions of a Ring Stiffened Cylindrical Shell.

[4]Almroth, B. O., and Brogan, F. A., and Stanley, G. M., Structural Analysis of General Shells, Vol. II, User Instruction for STAGSC, LMSC-D633873, Apr 1979.

[5]Moussouros, M., Comparisons of Static Collapse Predictions of a Ring Stiffened Cylindrical Shell.

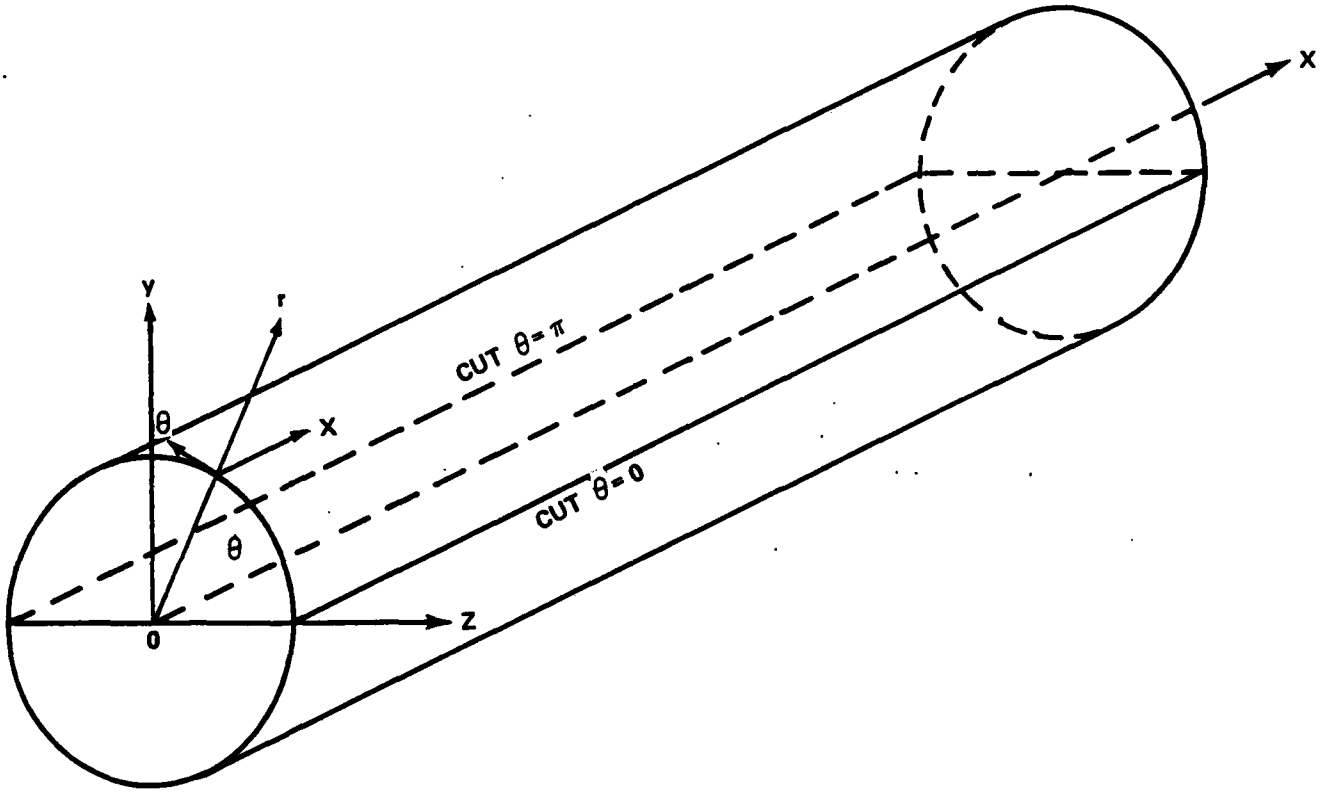

FIGURE 2. GLOBAL AND LOCAL FRAMES OF REFERENCE (s IS THE FRAME SPACING)

(3) Solutions by two alternative elements;

(4) Degradation of strength due to a hole; and

(5) The effect of initial imperfections on the computed critical pressure.

Comparisons with other sources and programs such as NASTRAN, are also included.

1. EFFECT OF BOUNDARY CONDITIONS IN THE MODELING PROCESS

We establish first two frames of reference, a global Cartesian (X,Y,Z) and a local cylindrical (r,θ,x). For convenience, the boundary conditions will be referred to the local system. Furthermore, we define the following terms pertaining to the boundary conditions:

(1) Type I (Symmetry):
$$U_x = 0$$
$$U_{\theta\theta} = 0$$
$$U_{rr} = 0$$

(2) Type II (Continuity):
$$U_{\theta\theta} = 0$$
$$U_{rr} = 0$$

(3) Type III (Symmetry):
$$U_\theta = 0$$
$$U_{xx} = 0$$
$$U_{rr} = 0$$

(4) Type IV (Antisymmetry):
$$U_x = 0 \quad \text{(No longitudinal translation)}$$
$$U_r = 0 \quad \text{(No radial translation)}$$
$$U_{\theta\theta} = 0 \quad \text{(No rotation about tangential axis)}$$

(5) Type V (Relaxed Antisymmetry):
$$U_r = 0$$
$$U_{\theta\theta} = 0$$

(6) Type VI (Horizontal Rigid Body Mode): At both $x=0$ and $x=3s$ and $\theta=\frac{1}{2}\pi$

$$U_\theta = 0$$

where s represents to frame spacing in the model

(7) Type VII (Horizontal Rigid Body Mode): At both x=0 and x=3s and $\theta=3\pi/2$

$$U_\theta = 0$$

(8) Type VIII (Vertical Rigid Body Mode): At both x=0 and x=3s and $\theta=0$ and $\theta=\pi$

$$U_\theta = 0$$

In order to investigate the effect of boundary conditions on the computation of the critical pressure, the following analyses have been carried out on a portion of a circular cylindrical shell encompassing three frame spaces (3s) and four equal T-stiffeners (rings): These models, referred to as models (1) - (5), are defined as follows:

(1) Full cylinder axially and peripherally with Type I boundary conditions on the first cross section and Type II on the second. To prevent vertical and horizontal rigid body motions, we apply boundary conditions of Type VI, VII, and VIII. (Boundary conditions (a) of Table 1.)

(2) Full cylinder axially, but only one half circumferentially with Type I boundary conditions on the first cross section and Type II on the second. At the generators, or cuts, $\theta = 0$ and $\theta = \pi$, apply Type III boundary conditions. To remove horizontal rigid body motion we use Type VI boundary conditions too. (Boundary conditions (b) of Table 1.)

(3) Full cylinder axially, but only one half peripherally with Type I and Type II boundary conditions at the two cross sections and Type III and Type IV at $\theta = 0$ and $\theta = \pi$. Also, apply Type VI conditions. (Boundary conditions (c) of Table 1.)

(4) Full cylinder axially, but only one half peripherally. Instead of Type IV conditions at $\theta = \pi$, as in Case (c), apply Type V conditions. (Boundary conditions (d) of Table 1.)

TABLE 1. CRITICAL BUCKLING PRESSURE FOR FULL OR HALF MODELS

Case	Type of Boundary Condition	Program Name	Bay No. 1 or 3		Bay No. 2		Element Type	Δp_{cr} (Lb/in^2)	Δp_1 (Lb/in^2)	Bay No. 2 Aspect Ratio
			No. of Axial Subdivisions	No. of Peripheral Subdivisions	No. of Axial Subdivisions	No. of Peripheral Subdivisions				
1	(a)	STAGS	2	24	4	24	410	263.38	293.74	3.60
2	(b)	STAGS	2	12	4	12	411	292.57	385.19	3.60
3	(c)	STAGS	4	12	8	12	411	198.27	255.62	7.20
4	(d)	STAGS	4	12	8	12	411	259.88	268.61	7.20
5	(e)	STAGS	4	12	8	12	411	261.29	268.20	7.20
6	(b)	STAGS	2	12	4	12	410	295.50	387.70	3.60
7	(b)	STAGS	4	12	8	12	410	286.05	310.41	7.20
8	(b)	STAGS	4	12	8	12	411	278.39	303.37	7.20
9	(b)	STAGS	4	24	8	24	410	440.71	667.66	3.61
10	(a)	STAGS	2	24	4	24	410	283.88	314.24	3.60
11	(b)	NASTRAN	2	12	4	12	QUAD 2	390.46	390.61	3.60

(5) Case (2) except that Type III conditions at the cuts $\theta = 0$ and $\theta = \pi$ are replaced by Type V. (Boundary conditions (e) of Table 1.) These are modified antisymmetry boundary conditions.

a. Description of Models

Model (1) was discretized using the STAGS 410 quadrilateral plate element with 6 D.O.F.*/node. The inplane translations normal to the edge were assumed linear, while the translations parallel to the edge were cubic. The out-of-plane deformation was taken as cubic. The first and third bays were discretized using 3 x 25 points, where 3 indicates the number of nodes axially, and 25, the number of nodes peripherally with $\theta = 15°$, and an aspect ratio ß, where

$$ß = \frac{2R \sin \{\theta/2\}}{\Delta x} = 9.0045/5 \simeq 1.8$$

and R is the shell radius, (34.50 in), Δx the element spacing axially (half a frame spacing) and $\theta = 15°$. The middle bay has a higher aspect ratio with $\Delta x = 2.5"$. Hence $ß = 3.6$.

Models (2) - (5) were analyzed using four axial subdivisions on the first and third bays and eight in the middle one. Circumferentially there were 13 points with the same aspect ratios and element type. In addition to the previous five cases, six additional combinations were also used. The last case (Case 11) is a NASTRAN computation with boundary conditions (b), similar to Case 6. Computed critical pressures are given on Table 1.

It is apparent that introducing antisymmetry at $\theta = \pi$, while maintaining symmetry at $\theta = 0$ (Case 3) (which incorporates the boundary condition $U_x = 0$ at $\theta = \pi$), lowers the critical pressure considerably from 292.57 Lb/in^2 to 198.27 Lb/in^2. This may result from the introduction of axial reaction forces at the antisymmetric side. This is further supported by the fact that for

*D.O.F. = Degrees of Freedom

Case 4, which omits the boundary condition $U_x = 0$ at $\theta = \pi$, for all x ($0 \leq x \leq 3s$) the critical pressure is increased to 259.8 Lb/in^2 from 198.27 Lb/in^2. Similar results follow for Case 5 with relaxed antisymmetry at both ends $\theta = 0$ and $\theta = \pi$.

The full versus half model comparisons (Cases 1 and 2, respectively) indicate a small reduction in the critical pressure from 292.57 Lb/in^2 (Case 2 and element type 411) (see also Reference 1) or 295.50 Lb/in^2 (Case 6 and element 410) to 263.38 Lb/in^2.

Table 1 also includes results for other combinations. Case 9, for example, differs from Case 7 in the aspect ratio. Mesh refinement to a more balanced aspect ratio results in bypassing the lowest eigenvalue, 286.05 Lb/in^2, and converges instead to 440.71 Lb/in^2. This is discussed later. The corresponding mode shapes for Cases 1-5 are given in Figures 2 through 11. As has already been mentioned, the model of Case 2 or 6 (which only differ in the plate element type) and is reported as Case 11 is run using NASTRAN. The critical pressure is obtained as 390.46 Lb/in^2. It is close to the circular ring solution reported in Table 2 as 391.63 Lb/in^2.

b. Effect of Initial Pressure

For all the above cases, the applied baseload pressure was 1 Lb/in^2. Case 1 was then recomputed using a baseload pressure of 100 Lb/in^2. The resulting critical pressure and modes were identical, suggesting independence of the result from this aspect of the procedure.

c. Effect of Live Load

For all cases reported here, unless otherwise noted, the pressure load was a "dead load," i.e., did not change direction of action. Case 1 (full model) was run with STAGS' "live load" option for pressure, yielding $\Delta p_{cr} = 280.14$ Lb/in^2 compared to the dead load result of 263.38 Lb/in^2. The corresponding critical mode was identical to that of Figure 2. Appendix A contains Tables A-1 and A-2 displaying the mode 1 displacement distributions for the dead and live pressures of Case 1.

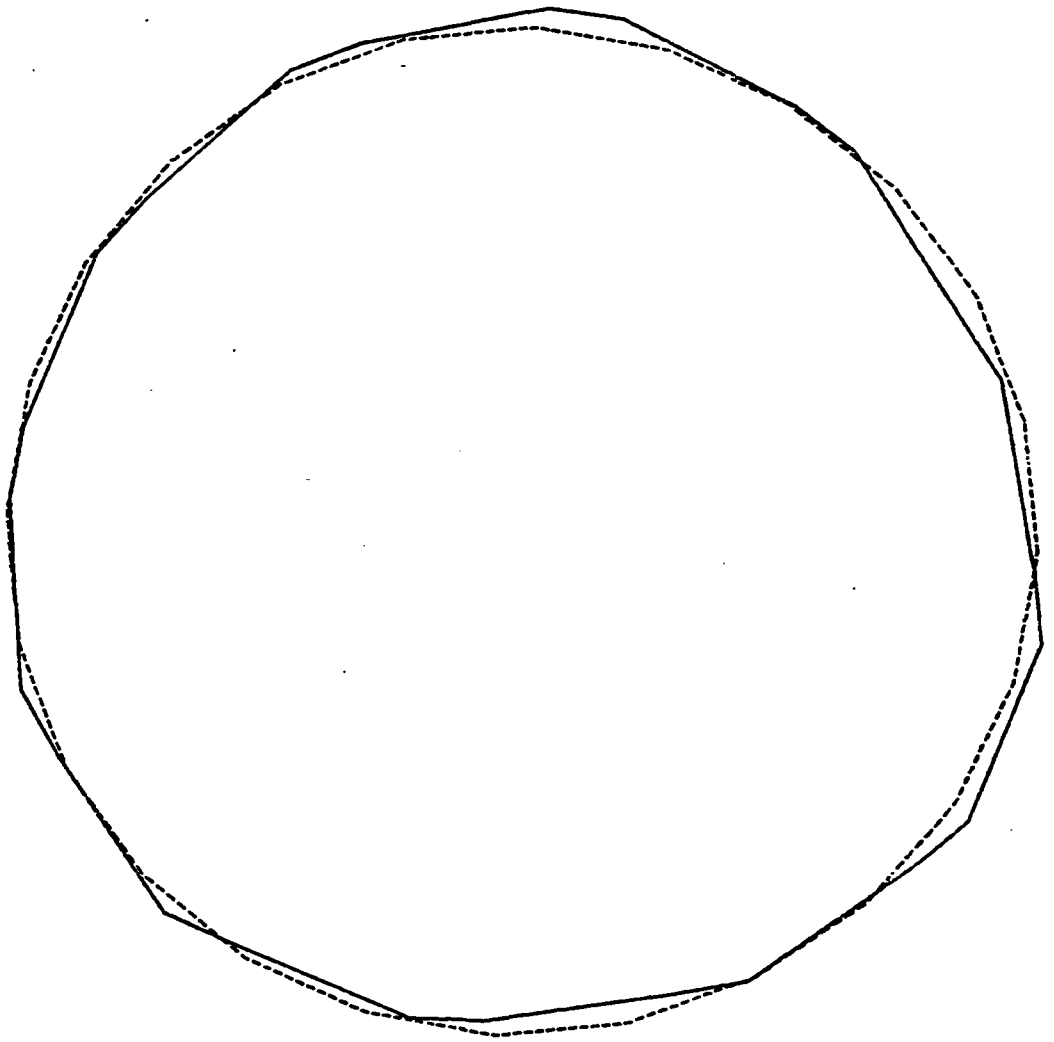

FIGURE 3. PLOT OF ORIGINAL FORM AND MODE 1 AT A CROSS SECTION AT x = 1.5s, CASE 1, MAGNIFICATION = 20,000

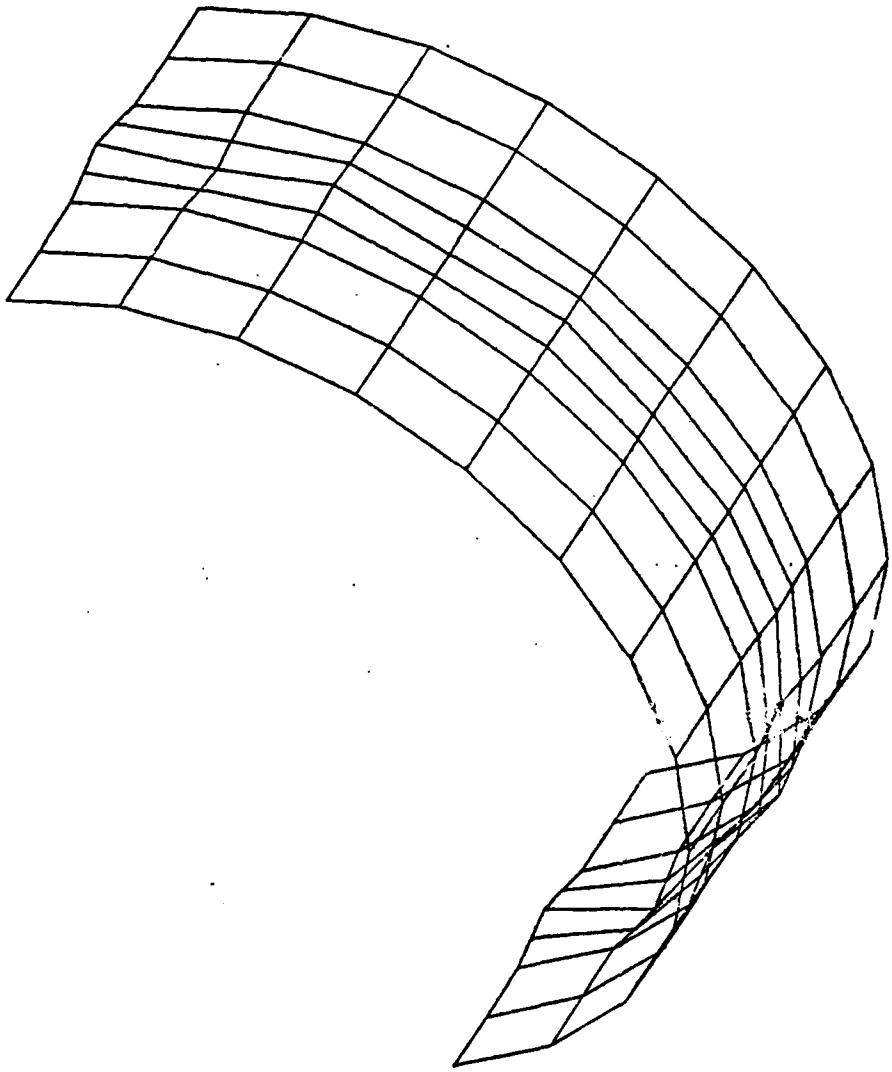

FIGURE 4. MODE 1 FOR CASE 2, HALF MODEL PERIPHERALLY, SYMMETRICAL BOUNDARY CONDITIONS, Δp_{cr} = 292.57 LB/IN^2

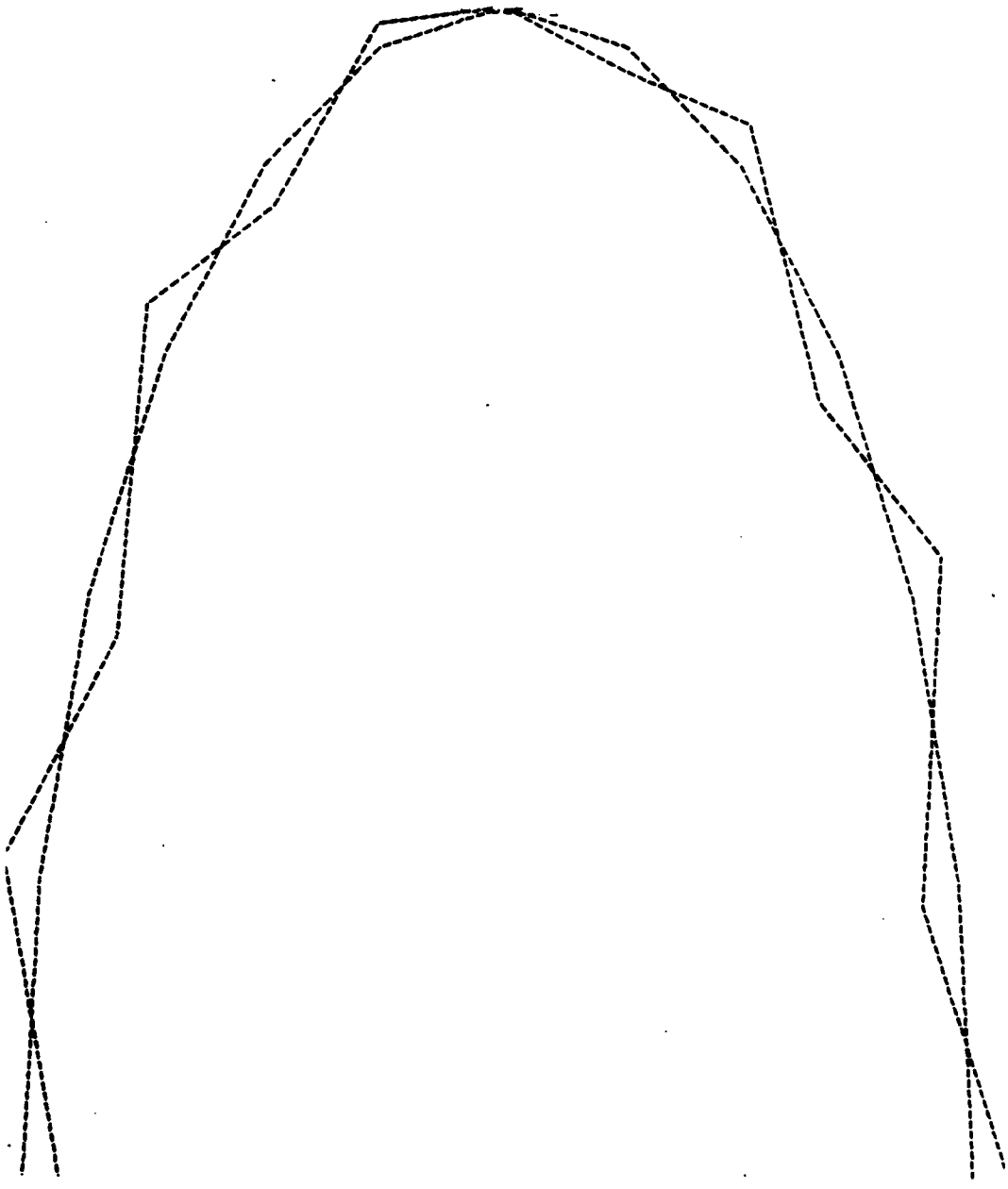

FIGURE 5. PLOT OF ORIGINAL FORM AND MODE 1 AT A CROSS SECTION AT x = 1.5s, CASE 2, VERTICAL SCALE IS TWICE HORIZONTAL, MAGNIFICATION = 4

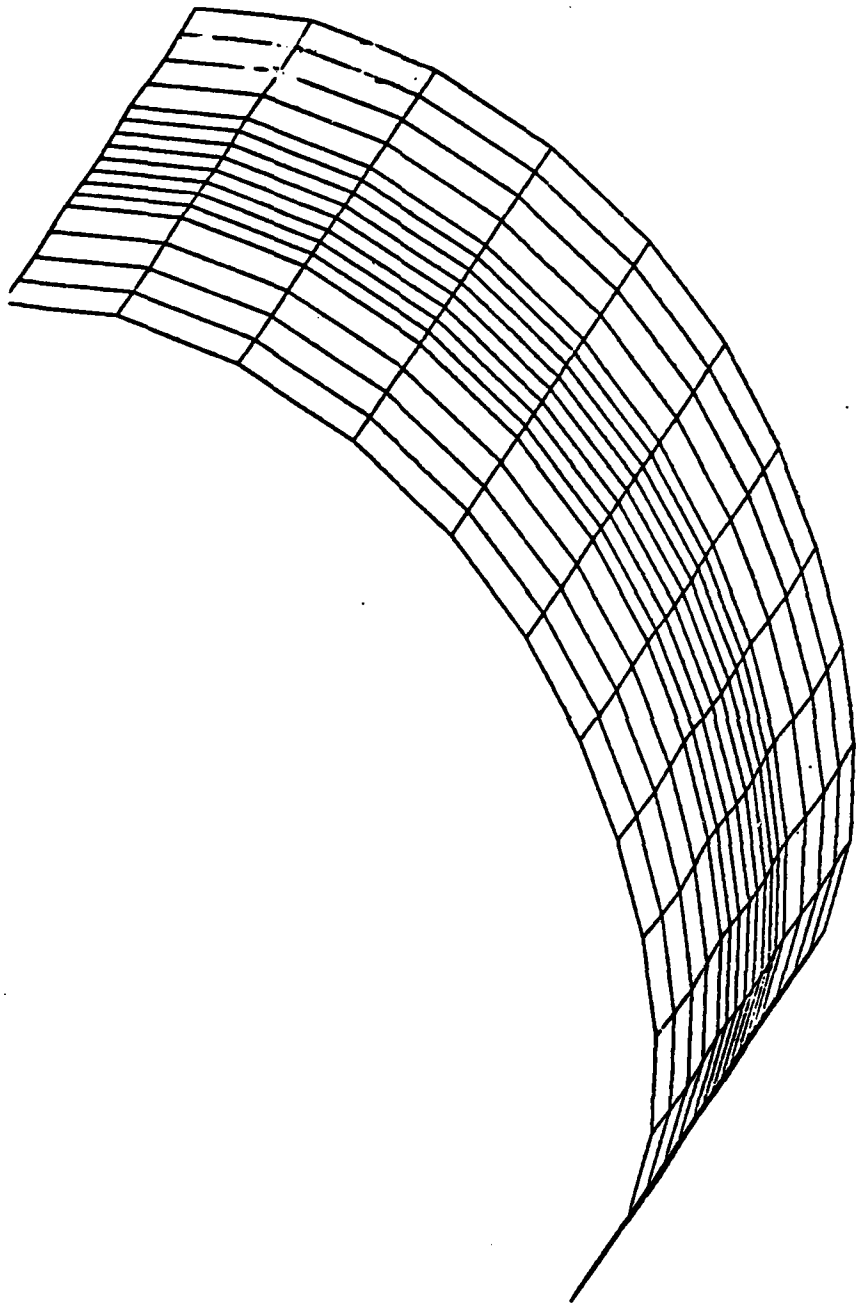

FIGURE 6. MODE 1 FOR CASE 3, HALF MODEL PERIPHERALLY, SYMMETRY AT $\theta = 0$, ANTISYMMETRY ($U_x = 0$) AT $\theta = \pi$

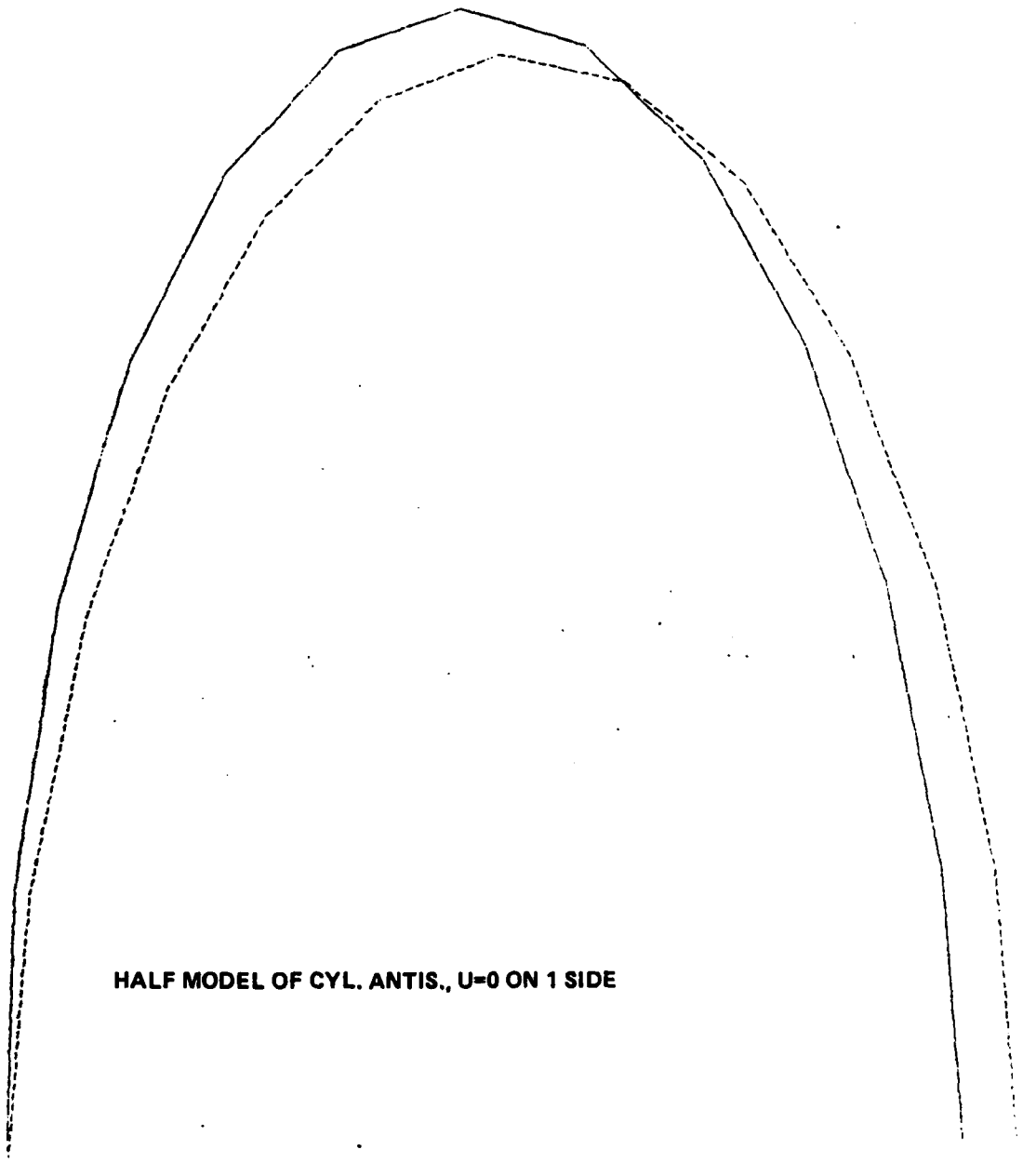

FIGURE 7. PLOT OF ORIGINAL FORM AND MODEL 1 AT A CROSS SECTION AT x = 1.5s, CASE 3, VERTICAL SCALE IS TWICE HORIZONTAL, MAGNIFICATION = 4

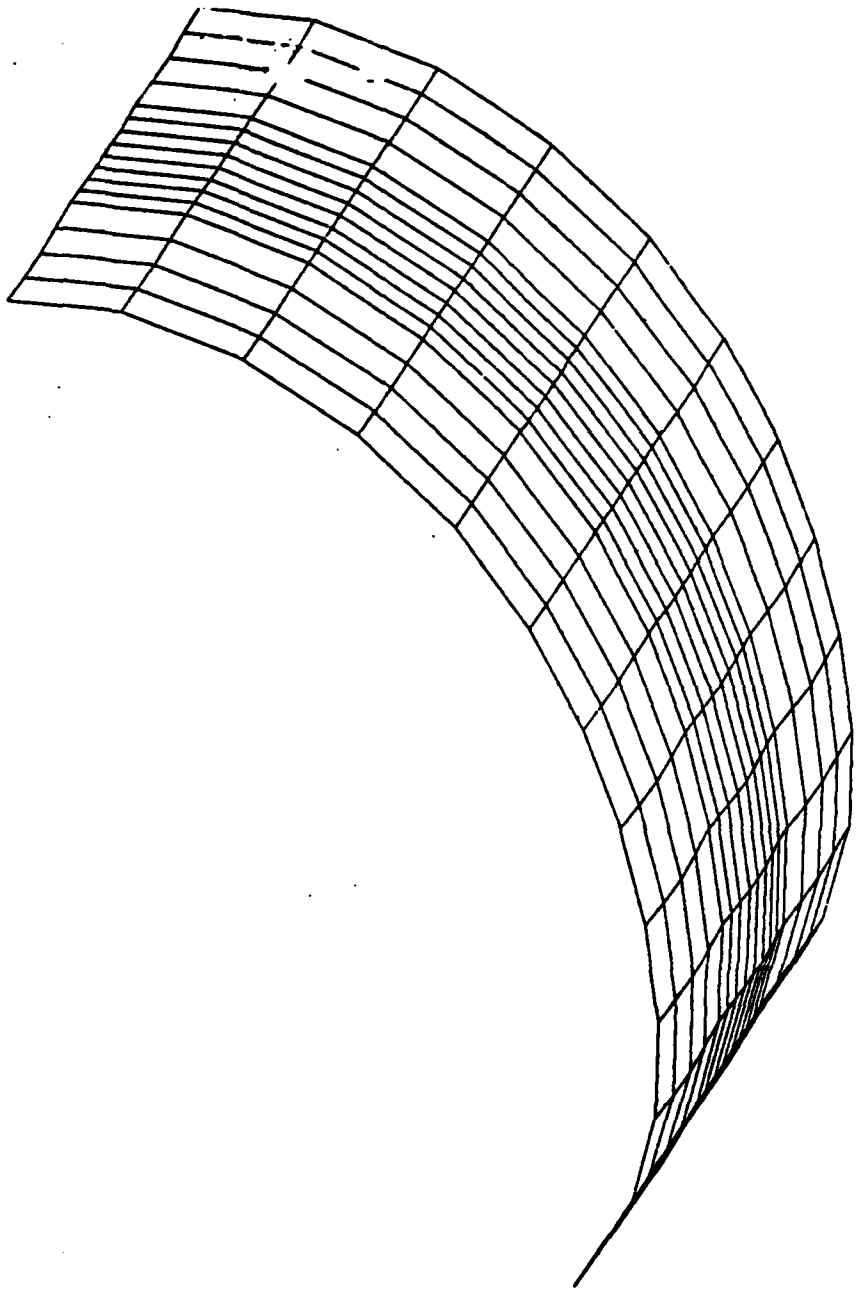

FIGURE 8. MODE 1 FOR CASE 4, HALF MODEL PERIPHERALLY, SYMMETRY AT $\theta = 0$, MODIFIED ANTISYMMETRY AT $\theta = \pi$ ($U_x \neq 0$), $\Delta p_{cr} = 259.88$ LB/IN^2

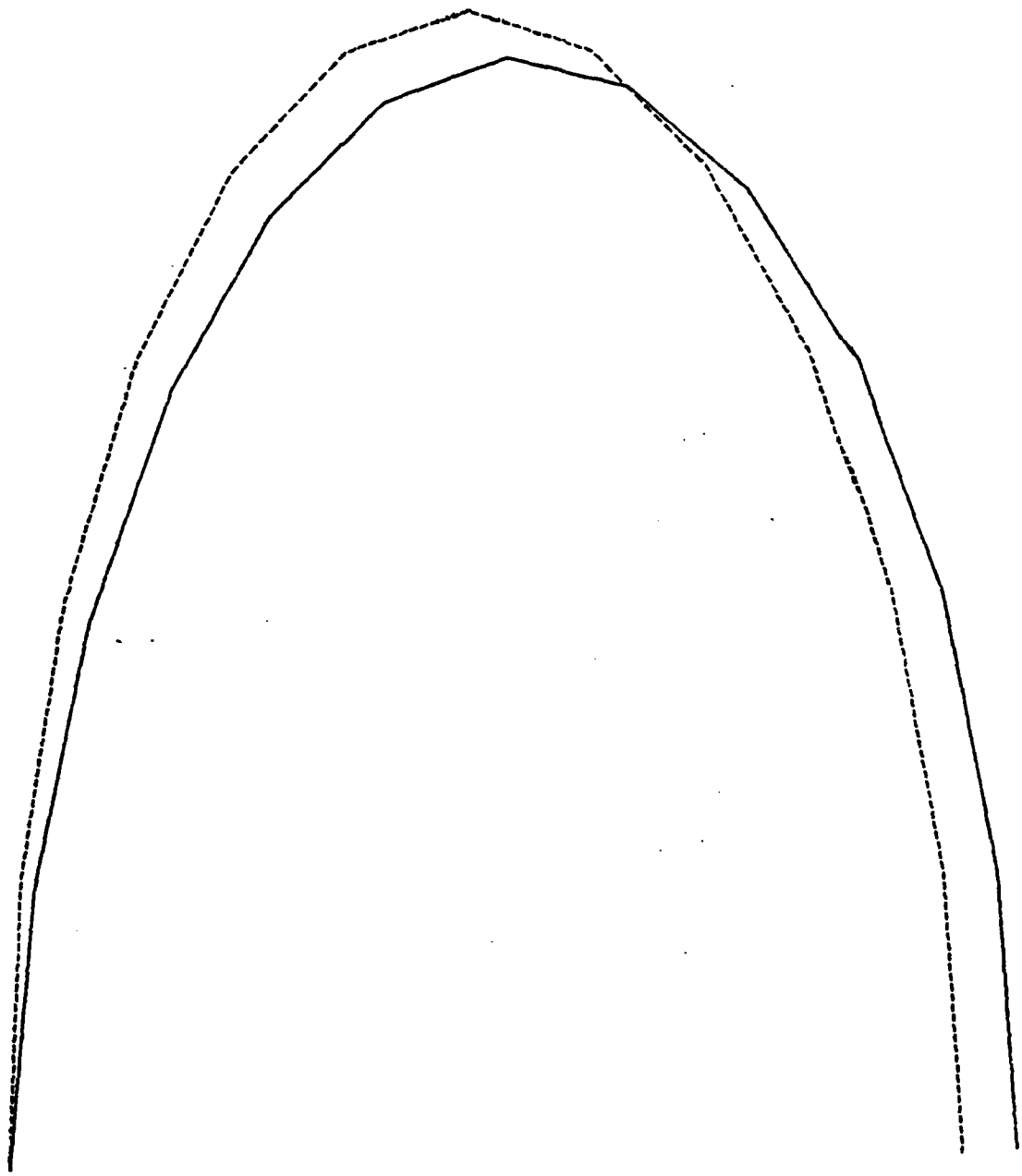

FIGURE 9. PLOT OF ORIGINAL FORM AND MODE 1 AT A CROSS SECTION AT x = 1.5s, CASE 4, VERTICAL SCALE IS TWICE HORIZONTAL, MAGNIFICATION = 4

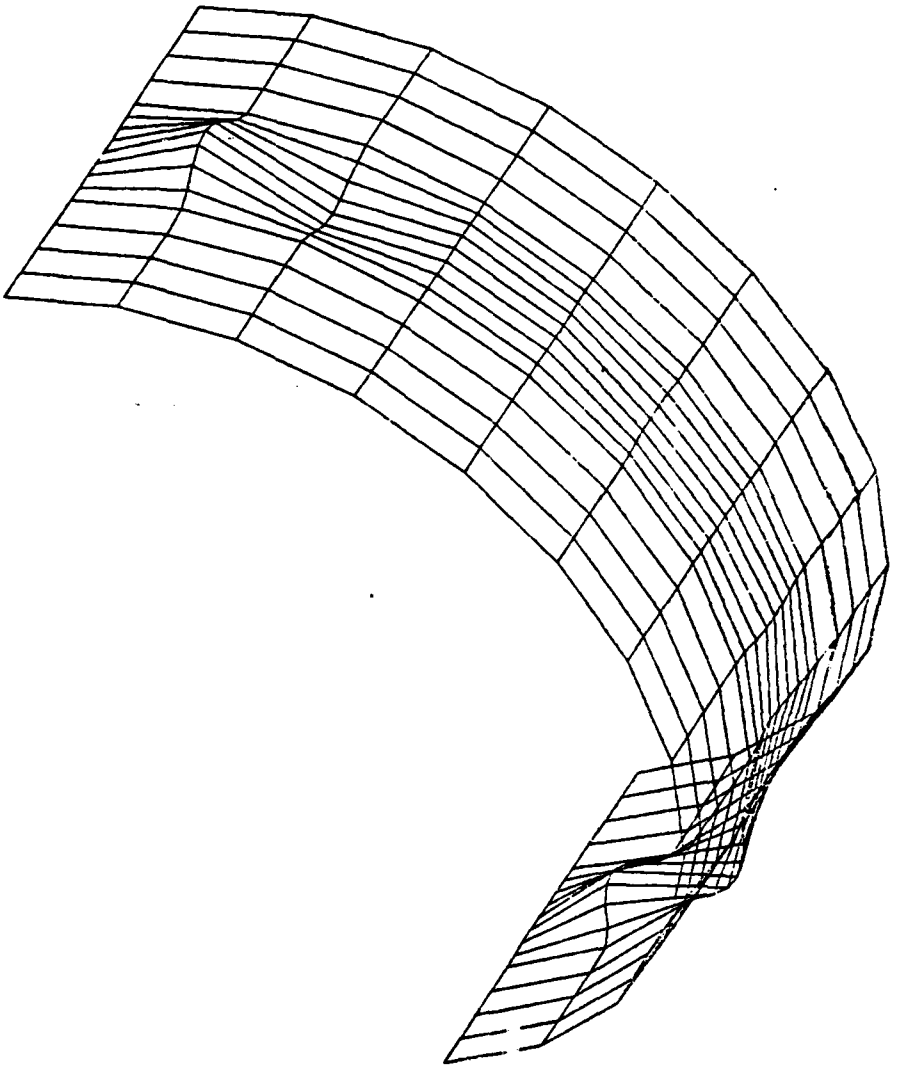

FIGURE 10. MODE 1 FOR CASE 5, HALF MODEL PERIPHERALLY, Δp_{cr} = 261.29 LB/IN^2

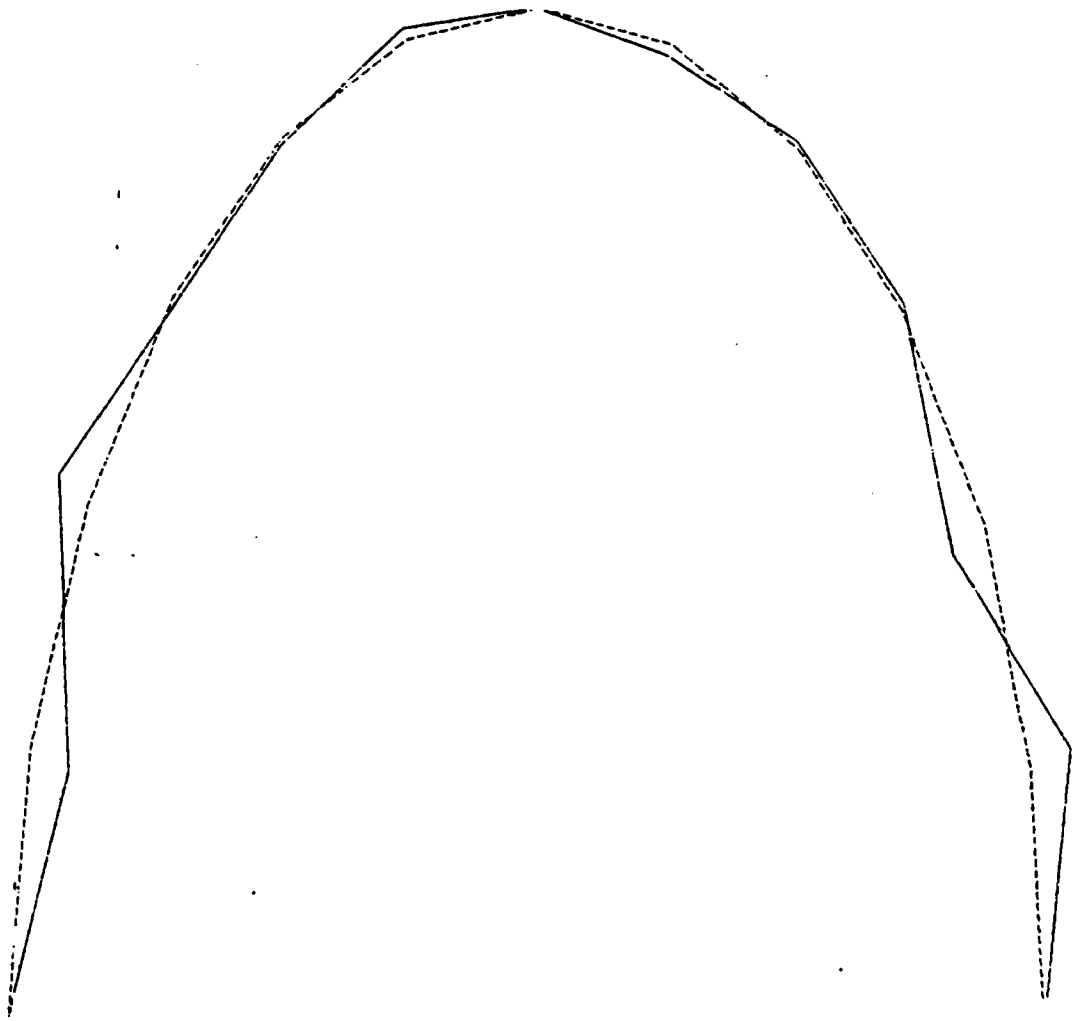

FIGURE 11. PLOT OF ORIGINAL FORM AND MODE 1 AT A CROSS SECTION AT x = 1.5s, CASE 5, MAGNIFICATION = 4

d. Mode Shapes

Examination of the mode shape corresponding to the calculated critical pressures suggests that the ring reinforced shell will buckle in an asymmetric, local, mode otherwise referred to as lobar or diamond-shape buckling. The known forms are: (1) Axisymmetric local buckling (combination of yielding and buckling), (2) Asymmetric local buckling in between the ring stiffeners, and (3) General Asymmetric buckling. These forms are displayed in Figures 12 through 14.* They correspond to bifurcation rather than limit points, as already mentioned.

e. Comparison with Other Computations

Table 2 is a summary of results obtained with a computer program based on various formulae for elastic buckling. We note that "Fluegge's formula"[6,7] is for general instability, while "Fluegge's formula (skin only)" is for interbay instability. Most of these results were reported in Reference 8, where they were calculated manually. These can also be compared with the NASTRAN result reported in Table 1 and discussed previously.

---

*Reproduced from Renzi, J. R., Optimization of Orthotropic, Non-Linear, Ring-Stiffened Cylindrical Shells Under External Hydrostatic Pressure as Applied to MMC Materials, NSWC TR 79-305, 30 Sep 1979.

[6]Fluegge, W., "Die Stabilitaet der Kreiszylinderschale," Ingenieur Archiv, Vol. 3, pp. 403-506, 1932.

[7]Timoshenko, S. P., and Gere, J. M., Theory of Elastic Stability (McGraw-Hill Book Co., Second Edition, 1961), pp. 457-519.

[8]Moussouros, M., Comparisons of Static Collapse Predictions of a Ring Stiffened Cylindrical Shell.

FIGURE 12. AXISYMMETRIC LOCAL BUCKLING

FIGURE 13. ASYMMETRIC LOCAL BUCKLING (LOBAR OR DIAMOND SHAPE BUCKLING)

FIGURE 14. GENERAL ASYMMETRIC BUCKLING

TABLE 2.

SUMMARY OF CRITICAL PRESSURES AS PER DIFFERENT METHODS IN THE OPEN LETERATURE

CIRCULAR RING FORMULA.	CRITICAL PRESSURE =	391.639	LB/SQ.IN.
R. VON MISES FORMULA.	CRITICAL PRESSURE =	494.266	LB/SQ.IN.
SOUTHWELLS FORMULA.	CRITICAL PRESSURE =	380.569	LB/SQ.IN.
U.S. EXP. MOD. BASIN FORMULA.	CRITICAL PRESSURE =	495.622	LB/SQ.IN.
FLUEGGES FORMULA.	CRITICAL PRESSURE =	2161.224	LB/SQ.IN.
FLUEGGES FORMULA (SKIN ONLY.)	CRITICAL PRESSURE =	494.230	LB/SQ.IN.

NOTE: Inertia of plate stiffener combination is calculated assuming full effectiveness, $I = 1.7869\ in^4$.

f. Stress State After Buckling

Examination of the resulting stresses corresponding to a critical pressure $\Delta p_{cr} = 263.68$ Lb/in^2 gives at midbay 2 a longitudinal stress $\sigma_{xx} \approx$ -24.15 ksi (i.e. 47% of yield), a circumferential stress $\sigma_{\theta\theta} \approx -37.92$ ksi (75% of yield) ($\sigma_{xx}/\sigma_{\theta\theta} \approx 0.637$), and a maximum stiffener stress, -20.62 ksi (40% of yield). The buckled configuration exhibited only elastic deformation.

g. Comments on Additional Computations

Additional computations have been performed using STAGSC to evaluate a method proposed by Brendel and Ramm.[9] According to these authors, one first obtains the approximate number of circumferential waves (m) through a formula such as

$$m = 2.742 \sqrt[4]{\frac{R^3}{L^2 h}}$$

or by using Figure 15. In the present case, the formula gives m = 17.54, while Figure 15 indicates either m = 14 or m = 15. For the model results reported below, the effects of ring stiffeners were incorporated using discrete beam elements.

These values are only approximate and it is, therefore, necessary to compute the minimum eigenvalue for a variety of angles, corresponding to m peripheral waves, and for suitable aspect ratios. Table 3, formed by computing θ segments from 18° to 180° (m = 20 to m = 2), indicates that m = 3 corresponds to the critical pressure, the magnitude of which agrees fairly well with the full and even the half models (Cases 1 and 2). There is, however, disagreement between the number of waves at buckling. Figure 3 and Table A-1 tend to support

---

[9]Brendel, B., and Ramm, E., "Linear and Nonlinear Stability Analysis of Cylindrical Shells," Journal of Computers & Structures, Vol. 12, pp. 549-558, 1980.

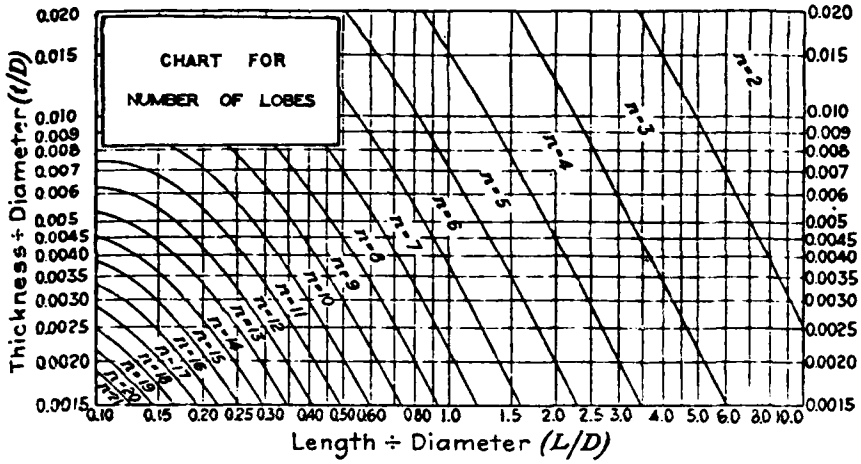

FIGURE 15. (h/D) RATIO AS A FUNCTION OF (ℓ /D) RATIO FOR VARIOUS NUMBER OF LOBES *

* *Reproduced from Windenberg, D. F., and Trilling, C., "Collapse by Instability of Thin Cylindrical Shells Under External Pressure," Transaction of ASME, Journal of Applied Mechanics, Vol. 56, No. 11, pp. 819-825, Nov. 1934.*

TABLE 3. BUCKLING ANALYSIS OF PANELS BETWEEN RING STIFFENERS

(m) No. of Waves Peripherally	$\theta(^o)$ [One Wave]	No. of Segments Peripherally	No. of Segments Axially	Aspect Ratio $\Delta s/\Delta x$	λ_{min} (Lb/in^2)
2	180	12	4	0.900	308.4
3	120	12	2	1.203	259.0
4	90	6	2	1.800	484.1
6	60	6	4	2.406	561.7
15	24	6	4	1.440	782.6
16	22.5	6	4	1.351	773.9
20	18	6	4	1.083	813.1

6 half waves over the entire ring (2 half waves over 120°) versus 1 half wave by the previous process. See Table A-3. Figure 16, which shows the mode 1 shape for a panel with an arc $\theta = 120°$ is very similar to that of Figure 2. Figure 17 shows mode 1 for the case of a panel $\theta = 90°$, assumed to contain 1 full wave. The computation indicates 5 half waves over the 90^{o} arc. On the face of it, the previous method may be unreliable as far as mode shape is concerned. It must be emphasized, however, that aspect ratio has a marked effect on the critical load and the corresponding mode as is evidenced in Table 4 for the panel analysis.

For most cases, except $\theta = 180°$ and 120°, as the aspect ratio goes up (number of circumferential elements versus axial ones), Δp_{cr} is reduced. Note that, if the aspect ratio is reduced considerably, the critical pressure increases substantially in the direction of that of a simply supported strut of length s* between ring stiffeners subject to axial loading.

2. EFFECT OF MESH REFINEMENT ON EIGENVALUES

The following discussion, though not comprehensive, appears to be generally applicable. (See Table 5.) That is, a refinement of the mesh in the circumferential direction (increase of aspect ratio from 3.60 to 7.20) lowers the computed eigenvalue from 295.00 Lb/in^2 to 286.86 Lb/in^2 (Case 1 to Case 2). Refinement by increasing the number of elements by a factor of two (Case 1 to Case 3), while maintaining essentially the same aspect ratio, leads to confusing results. It appears that mesh refinement tends to increase the dimensionality of the problem to the point at which accurate extraction of the lowest eigenvalue becomes difficult.

---

*$\sigma_{CR} = \frac{\pi^2}{12} E(\frac{h}{s})^2 = \frac{\pi^2}{12} \times 30 \times 10^6 \times (\frac{0.245}{10})^2 = 14{,}810\ Lb/in^2$

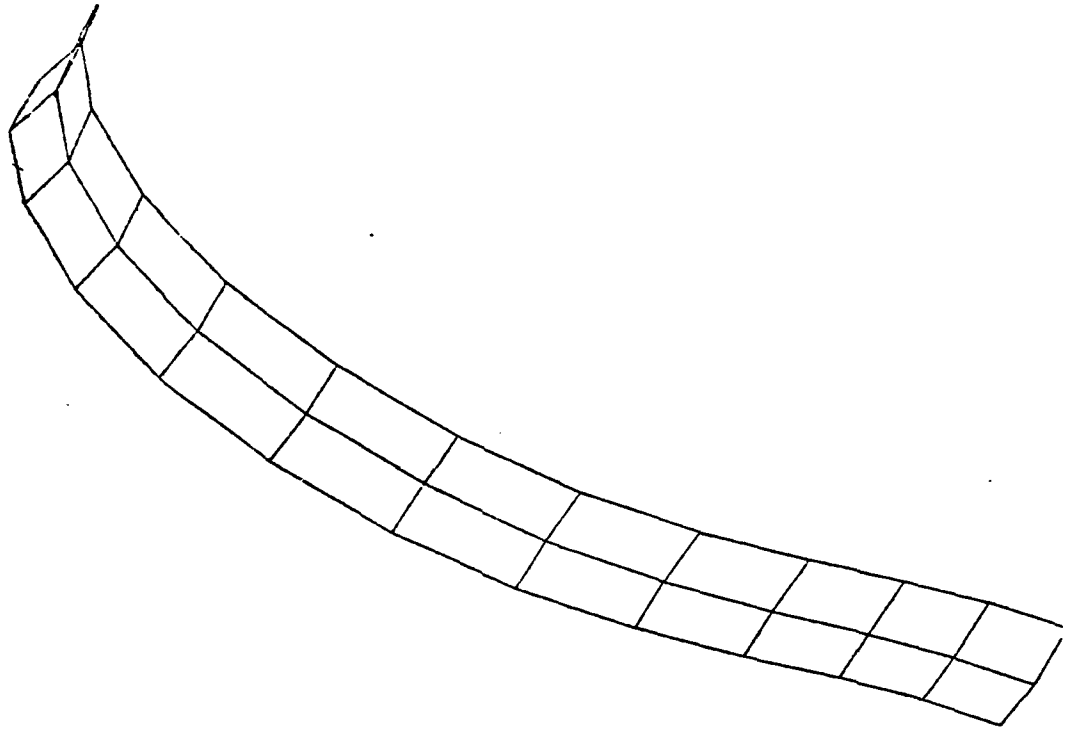

FIGURE 16. MODE 1 OF PANEL WITH ARC $\theta = 120^{o}$, 3 x 13 POINTS ENCOMPASSING 3 WAVES

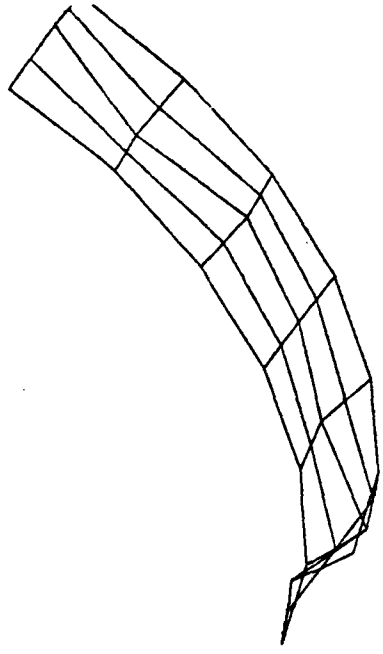

FIGURE 17. MODE 1 OF A PANEL OF ARC $\theta = 90^{o}$, 5 x 7 POINTS ENCOMPASSING 4 WAVES

TABLE 4.

BUCKLING ANALYSIS OF PANELS BETWEEN RING STIFFENERS FOR A RANGE OF ASPECT RATIOS

No. of Waves Peripherally	θ(°) [one wave]	No. of Segments Peripherally	No. of Segments Axially	Aspect Ratio $\Delta s/\Delta x$	λmin (lb/in^2)
2	180	6	2	3.60	137.79
2	180	12	2	1.80	398.7
2	180	12	4	0.90	308.4
3	120	6	2	2.40	271.7
3	120	12	2	1.20	259.0
4	90	6	2	1.80	484.1
4	90	6	4	3.60	407.8
6	60	6	4	2.40	561.7
6	60	6	2	1.20	1,116.5
6	60	12	2	0.60	1,089.5
12	30	6	2	0.60	2,862.9
12	30	12	2	0.30	2,965.0
15	24	6	4	1.44	782.6
15	24	12	2	0.24	2,735.2
16	22.5	6	4	1.35	773.9
16	22.5	12	2	0.22	2,650.3
20	18	6	4	1.08	813.1
20	18	12	2	0.18	2,343.9

TABLE 5. EFFECT OF MESH REFINEMENT (6 D.O.F./NODE)

Case No.	Type of Boundary Condition	Total D.O.F	Aspect Ratio In Bay No. 2	Element Type	Δp_{cr} (lb/in^2)
1	(b)	702	3.60	410	295.00
2	(b)	1326	7.20	410	286.05
3	(b)	2550	3.61	410	440.71

3. SOLUTIONS BY ALTERNATIVE ELEMENTS

The present version of STAGSC offers a choice between plate elements series 410, 411, 412 and 420, 421, 422. Since we have already used 410, we employed 411 as a comparison. The quadrilateral plate element 411 has 32 D.O.F. with 3 translations, 2 inplane rotations, 2 independent normal rotations at each corner, and 1 tangential displacement at each mid-side node.[10] From Reference 11 it is evident that there are difficulties with the use of finite elements in instability phenomena. A case similar to Case 2 (Table 5), for the aspect ratio displayed on Table 1 as Case 2, and employing the 411 element was run. The results using these different elements were comparable (295.00 Lb/in^2 versus 292.57 Lb/in^2). On the face of it, it appears that for the type of problem considered, element 410 is, perhaps, more than sufficient, and the additional expense of the extra D.O.F. of element 411 is not warranted.

---

[10] Thomas, K., and Sobel, L. H., Evaluation of the STAGSC - 1 Shell Analysis Computer Program, Westinghouse Electric Corporation, Report N. Ward-10881, Aug 1981.

[11] Almroth, B. O., and Brogan, F. A., "Computational Efficiency of Shell Elements," AMD-Vol. 48, Nonlinear Finite Element Analysis of Plates and Shells, The American Society of Mechanical Engineers, Washington, D.C., 15-20 Nov 1981.

4. DEGRADATION OF STRENGTH DUE TO A HOLE

References 12 and 13 include some results of structures with holes. In the present analysis, the half model was studied with a cutout on one side only. The hole dimensions were $\Delta x * \Delta s$. The actual peripheral dimension in the cutout is $2\Delta s$. Computed results, employing element 410, indicate that there is a reduction in the elastic buckling load with holing. This is consistent with results of Reference 14. Table 6 summarizes these results. Examination of this Table suggests the danger of using non-uniform meshes in such computations as the lowest eigenvalue may be missed (Case 4). Although not fully conclusive, the first and second cases indicate a reduction in strength by 5% because of the hole. As the size of the opening is increased (from Case 1 to 2 and to 3) the critical pressure is reduced correspondingly. Figures 18-20 show the mode shapes for Case 2, while Figures 21 and 22 exhibit the critical mode shape for Case 3. Finally, the hole has a mild effect on the stress redistribution with the appearance of a small shear stress $\sigma_{x\theta}$ and an approximate magnification of longitudinal stresses by 1.5% and circumferential ones by 3.5%.

5. THE EFFECTS OF IMPERFECTIONS ON CRITICAL PRESSURE

A few numerical analyses have been carried out with the imperfections option of STAGS whereby the magnitude of the amplitude (W_o), the location of the maximum amplitude (X,θ), and half wave lengths of the imperfection axially (X_L) and tangentially (θ_L) were taken as

---

[12] Brogan, F., and Almroth, B. O., "Buckling of Cylinders with Cutouts," AIAA Journal, Vol. 8, No. 2, pp. 236-240, Feb 1970.

[13] Brogan, F. A., and Almroth, B. O., "Practical Methods for Elastic Collapse Analysis for Shell Structures," AIAA Journal, Vol. 9, No. 12, pp. 3421-2326, Dec 1971.

[14] Brogan, F., and Almroth, B. O., "Buckling of Cylinders with Cutouts.".

TABLE 6.

EFFECTS OF CUTOUTS ON CRITICAL PRESSURE

Case	Type of Model	Element Type	Half Opening Size $\Delta x * \Delta s$ (in x in)	Δp_{cr} (lb/in^2)
1	Same as Case 7, (5 x 13), No opening	410	0 x 0	286.05
2	Half model with symmetry at $\theta = o$, $\theta = \pi$. Uniform mesh in middle portion and twice as fine at ends (5 x 13)	410	2.5 x 9.032	272.94
3	Same as Case 2 (3 x 13)	410	5.0 x 9.032	266.26
4	Half model with symmetry at $\theta = o$, $\theta = \pi$. Nonuniform mesh peripherally and axially	410	0.50 x 0.25	374.96

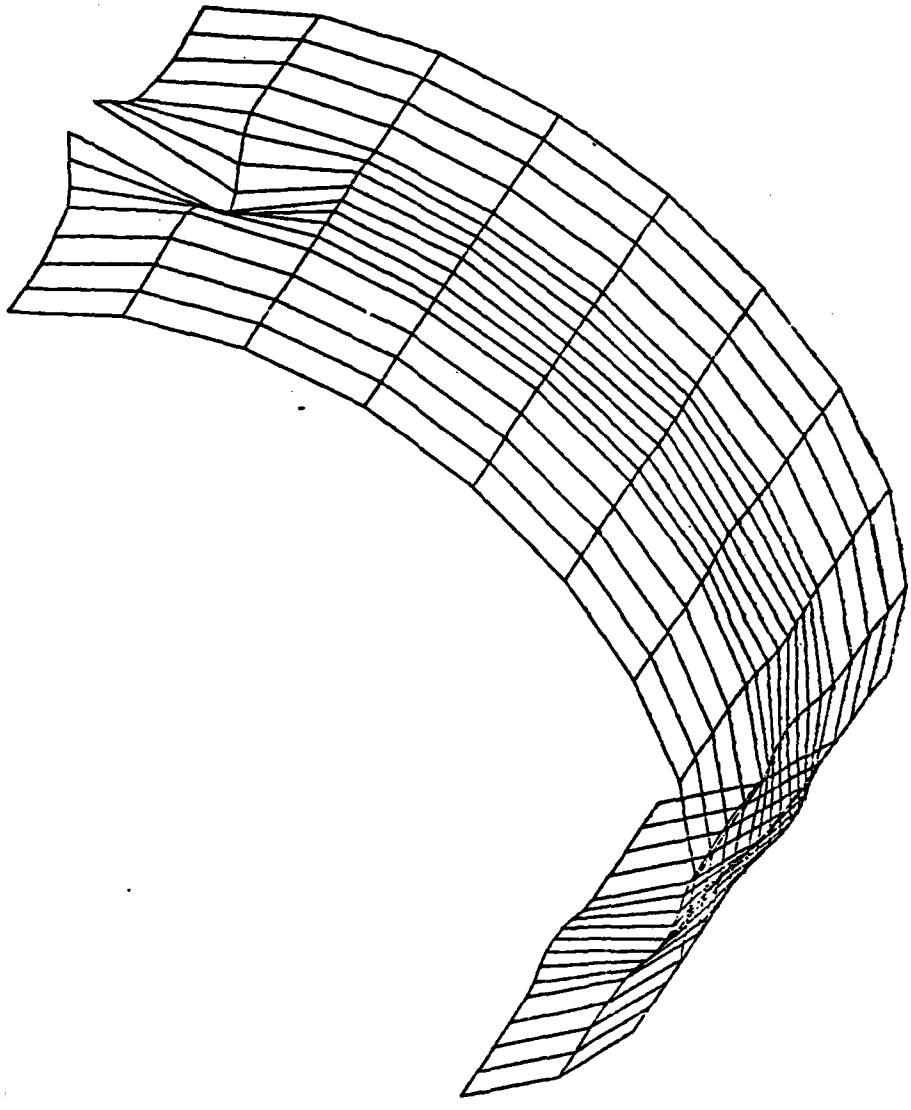

FIGURE 18. MODE 1 OPENING SIZE: $\Delta x = 2 \times 1.25$ IN, $\Delta s = 9.0045$ IN, $\Delta p_{cr} = 272.94$ LB/IN^2

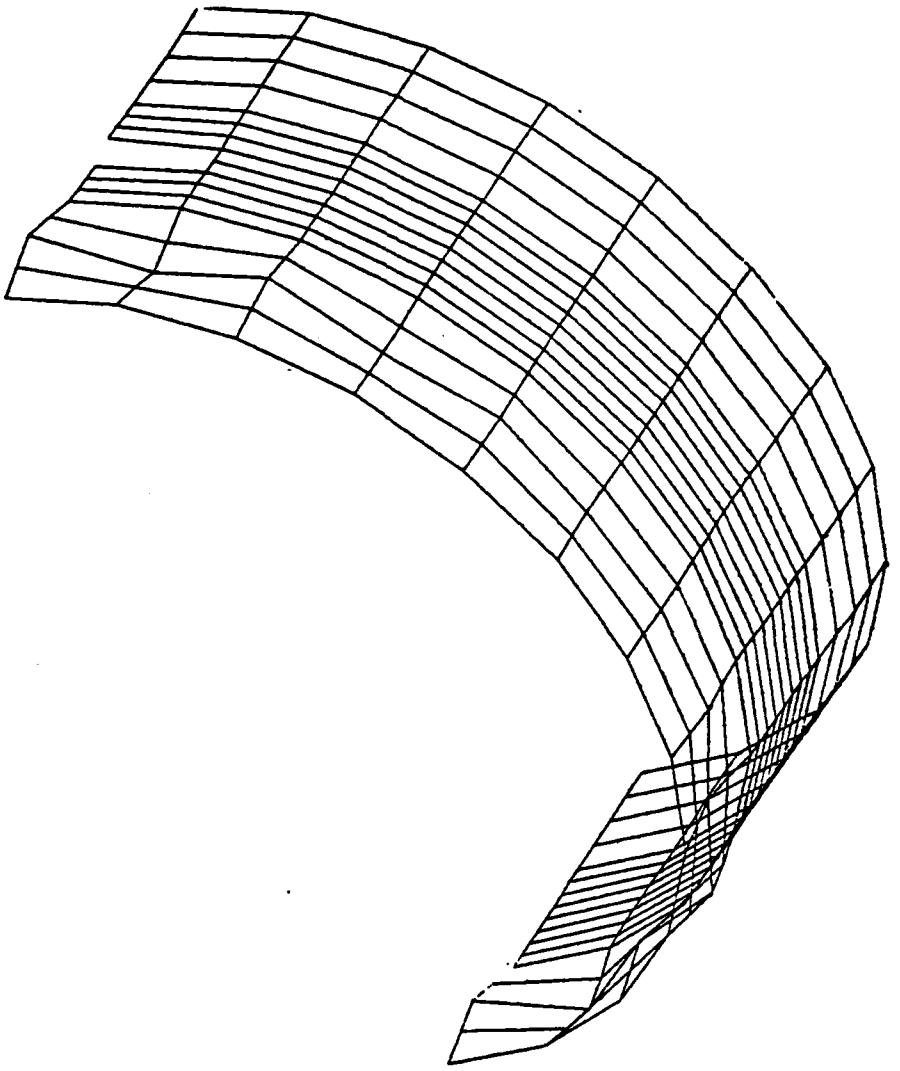

FIGURE 19. MODE 2 OPENING SIZE: $\Delta x = 2 \times 1.25$ IN, $\Delta s = 9.0045$ IN, $(\Delta p)_2 = 308.45$ LB/IN^2

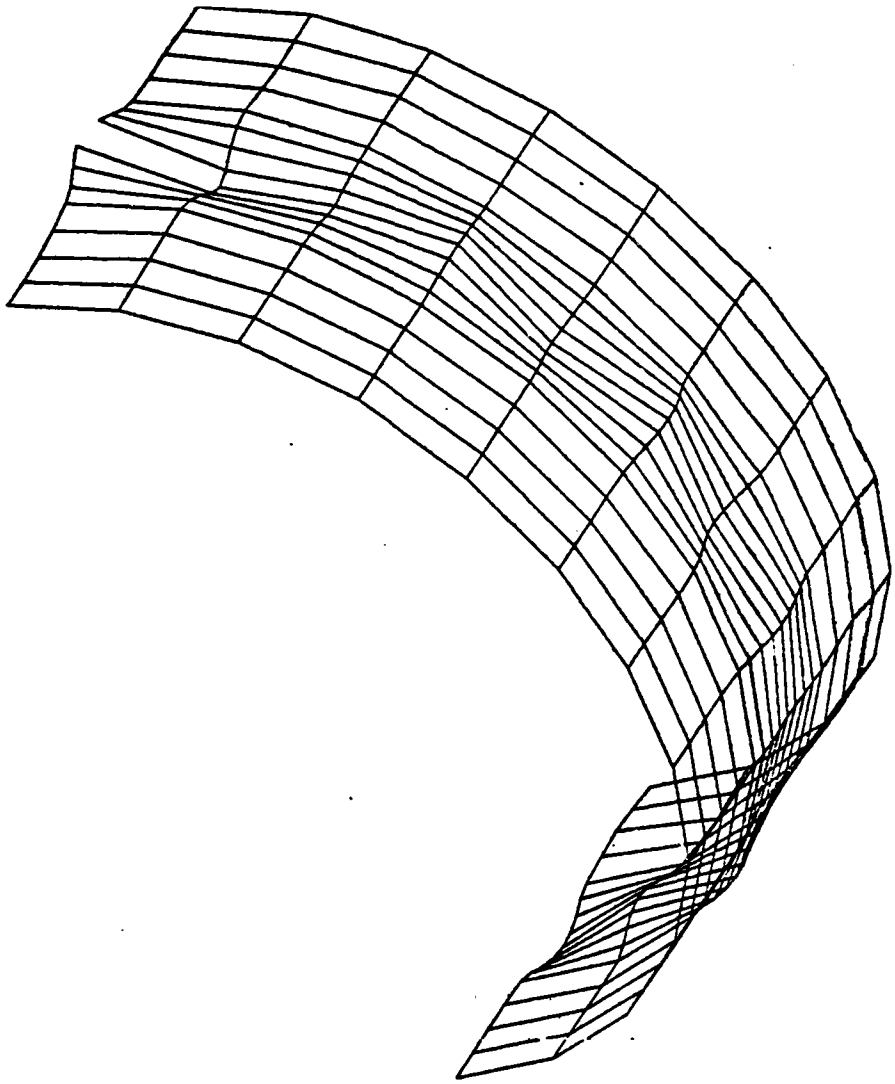

FIGURE 20. MODE 3 OPENING SIZE: $\Delta x = 2 \times 1.25$ IN, $\Delta s = 9.0045$ IN, $(\Delta p)_3 = 308.84$ LB/IN^2

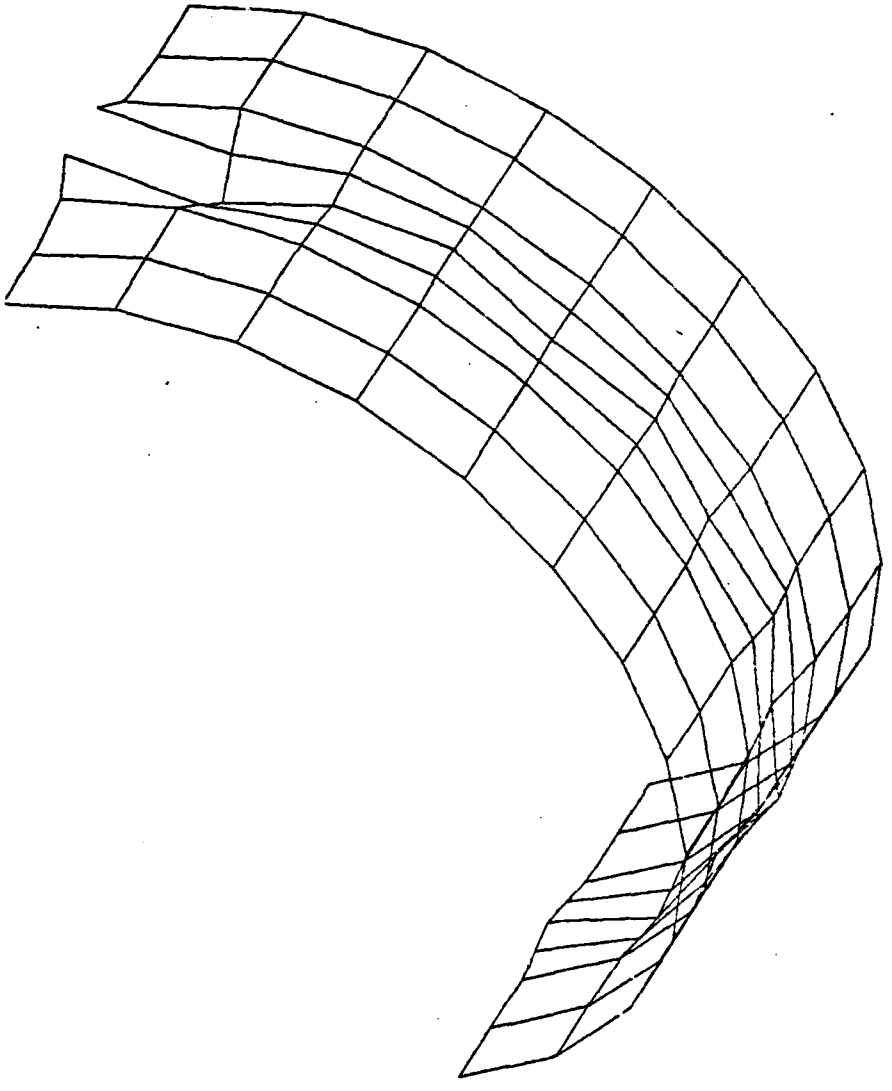

FIGURE 21. STIFFENED CYLINDRICAL SHELL WITH OPENING, NO IMPERFECTIONS, 3 x 13 MESH IN EACH BAY, (w) RADIAL DEFORMATION MODE, Δp , = 66.26 LB/IN^2

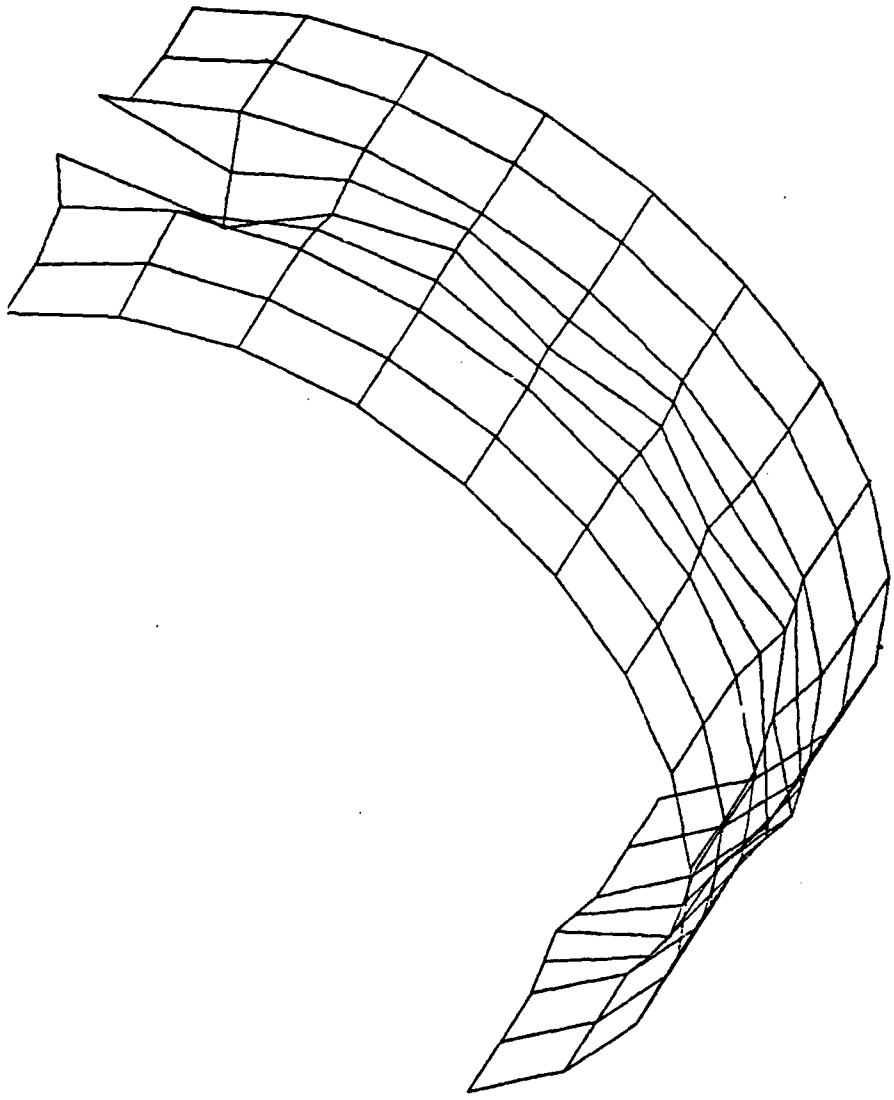

FIGURE 22. STIFFENED CYLINDRICAL SHELL WITH OPENING. (SAME AS FIGURE 21.) COMBINED DISPLACEMENTS (u, v, w) MODE, $\triangle p_{cr}$ = 266.26 LB/IN^2

$$W_o = 0.1h = 0.0245 \text{ in.}, \quad X_L = s = 10 \text{ in.}, \quad \theta_L = \frac{360}{36} = 10°$$

and

$$X = 1.5s = 15 \text{ in.}, \quad \theta = 0 \text{ in Cases 1, 2, } \theta = 10° \text{ in Case 3.}$$

The results are shown in Table A-1. Figures 23 through 27 display the corresponding critical mode for the case analyzed.

We can further investigate this question using results from Budiansky and Amazigo[15] and Bushnell[16] relating to asymptotic theory. In fact, using Figure 28 for the corresponding Batdorf non-dimensional parameter

$$Z = \frac{L^2}{Rh}\sqrt{1-\nu^2},$$

with L = 10 in, R = 34.5 in, h = 0.245 in, ν = 0.300, Z = 11.285, and with hydrostatic pressure and ring stiffeners, we obtain parameter b ≈ - 0.364. Since W_o = 0.1h = 0.0245 in. the Bushnell formula, where ΔP_s is the collapse pressure with imperfections, and ΔP_c of the ideal structure, is

$$\frac{\Delta P_s}{\Delta P_c} = 1-3\left(-\frac{b}{4}\right)^{1/3} \rho W_o$$

and assuming ρ = 1, we obtain

$$\frac{\Delta P_s}{\Delta P_c} = 0.886$$

which is about the same value obtained by using Figure 29. This results in a critical pressure ΔP_s = 261.8 Lb/in^2, using ΔP_c = 295.5 Lb/in^2 without the

---

[15]Budiansky, B. E., and Amazigo, J. C., "Initial Post-buckling Behavior of Cylindrical Shells Under External Pressure," Journal of Mathematics and Physics, Vol. 47, pp. 223-235, 1968.

[16]Bushnell, D., "Buckling of Shells-Pitfalls for Designers," AIAA Journal, Vol. 19, No. 9, pp. 1183-1226, Sep 1981.

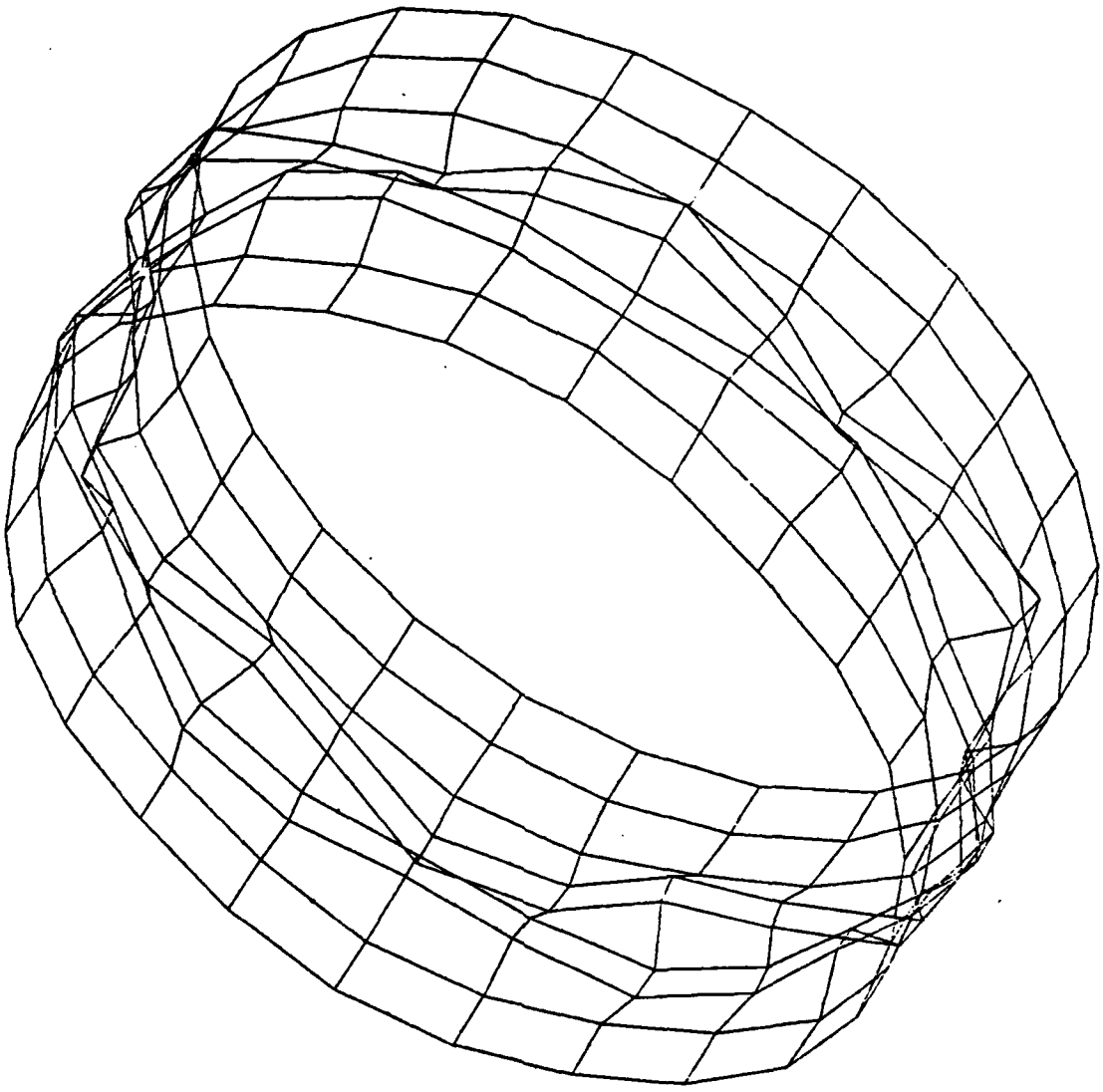

FIGURE 23. FULL STIFFENED CYLINDRICAL SHELL WITH IMPERFECTIONS. (u, v, w) COMBINED DEFORMATION MODE. AMPLITUDE OF IMPERFECTION = 0. 1h. MAXIMUM IMPERFECTION AMPLITUDE AT $x = 1.5s$, $\theta = 0$, $\Delta p_{cr} = 283.88$ LB/IN^2

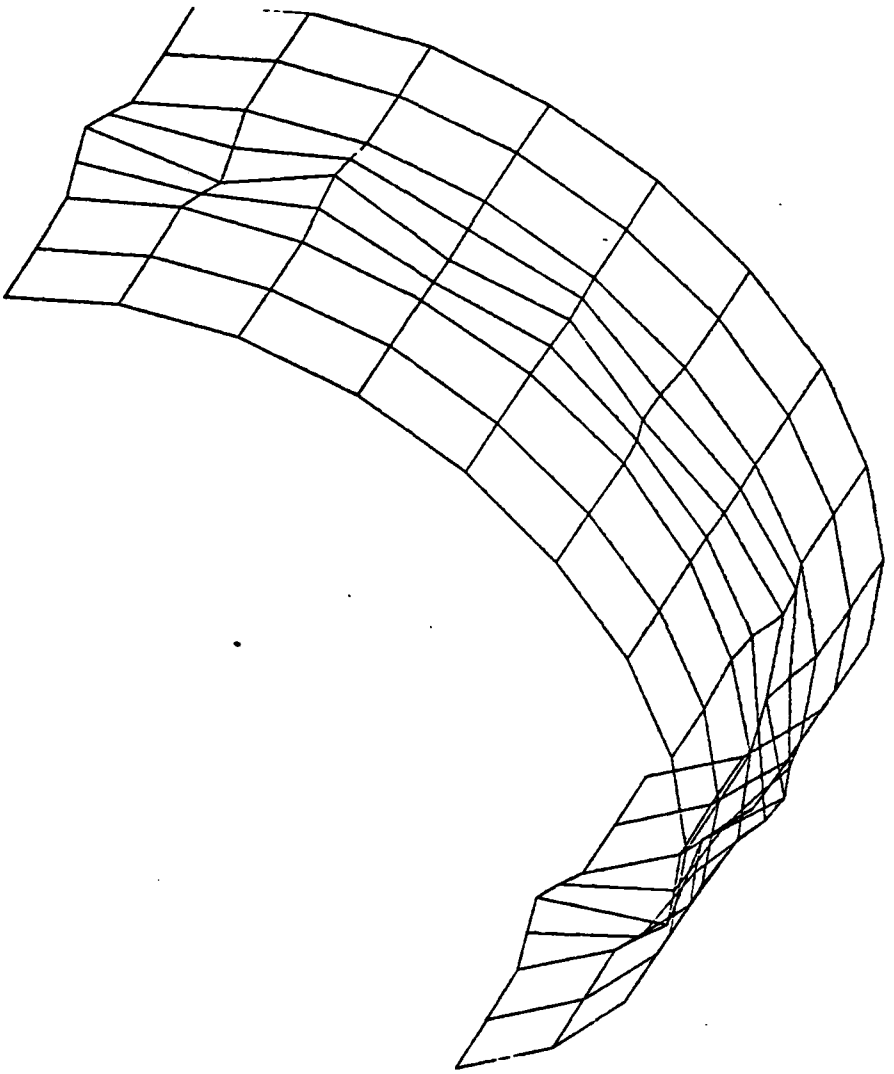

FIGURE 24. STIFFENED CYLINDRICAL SHELL. SYMMETRY CONDITIONS AT $\theta = 0$, $\theta = \pi$. (w) RADIAL DEFORMATION MODE. IMPERFECTION AMPLITUDE = 0.1h. MAXIMUM IMPERFECTION AT $x = 1.5s$, $\theta = 0$, $\Delta p_{cr} = 316.04$ LB/IN^2

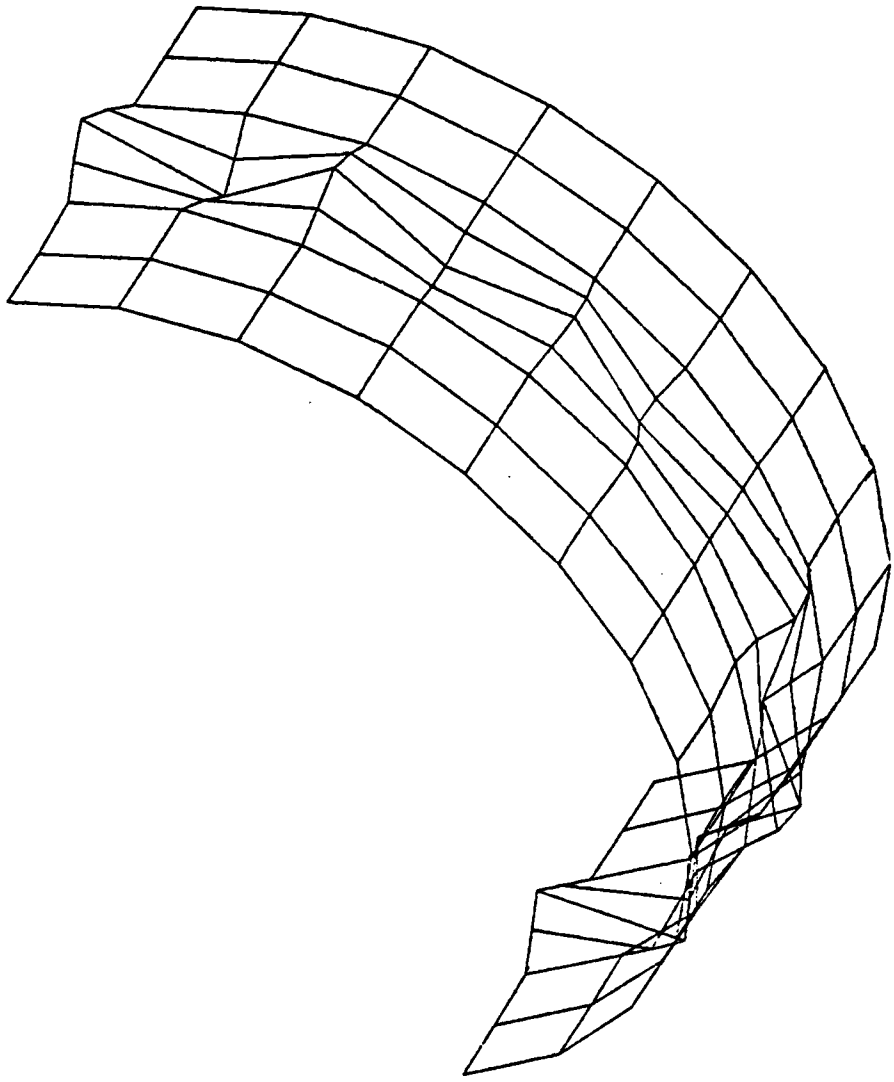

FIGURE 25. STIFFENED CYLINDRICAL SHELL. SAME AS FIGURE 24 COMBINED (u, v, w) DEFORMATION MODE. Δp_{cr} = 316.04 LB/IN^2

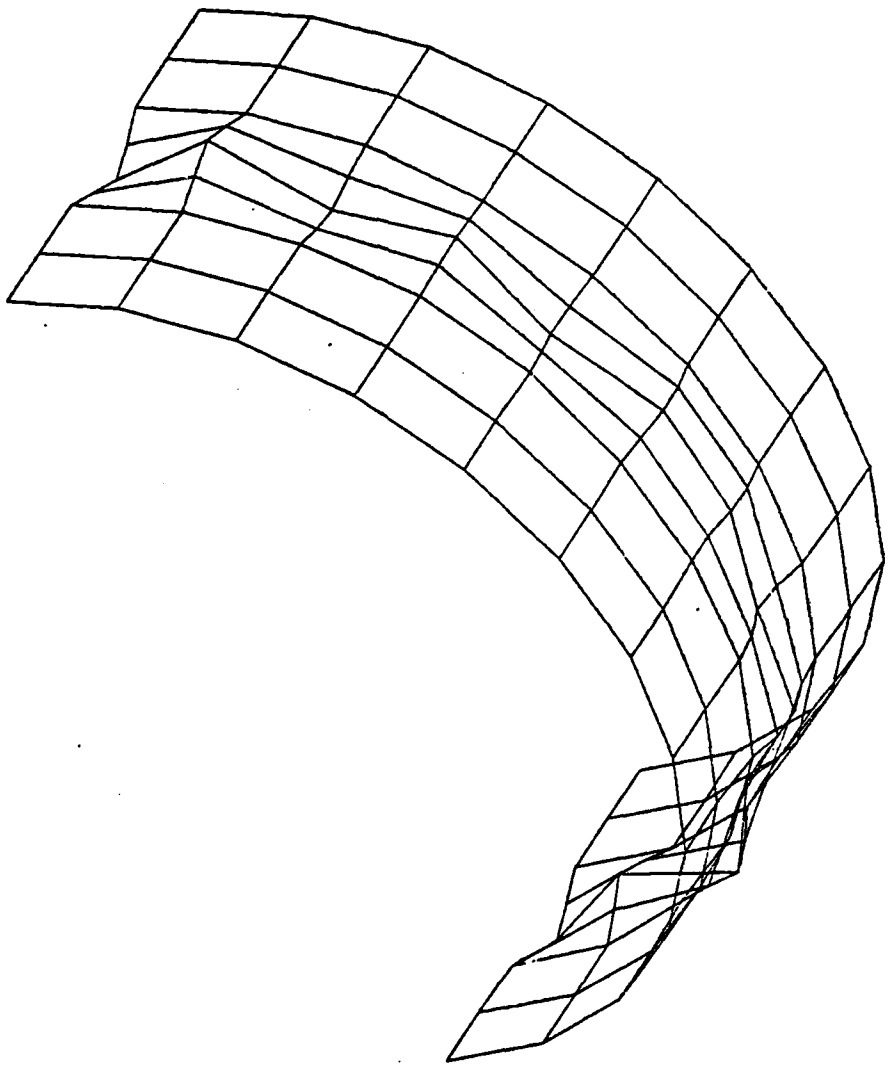

FIGURE 26. STIFFENED CYLINDRICAL SHELL WITH IMPERFECTIONS. SYMMETRY CONDITIONS AT $\theta = 0$, $\theta = \pi$. (w) RADIAL DEFORMATION MODE. IMPERFECTION AMPLITUDE = 0. 1 h. MAXIMUM IMPERFECTION AMPLITUDE AT x = 1.5s, $\theta = 10^{o}$, $\Delta p_{cr} = 316.04$ LB/IN^2

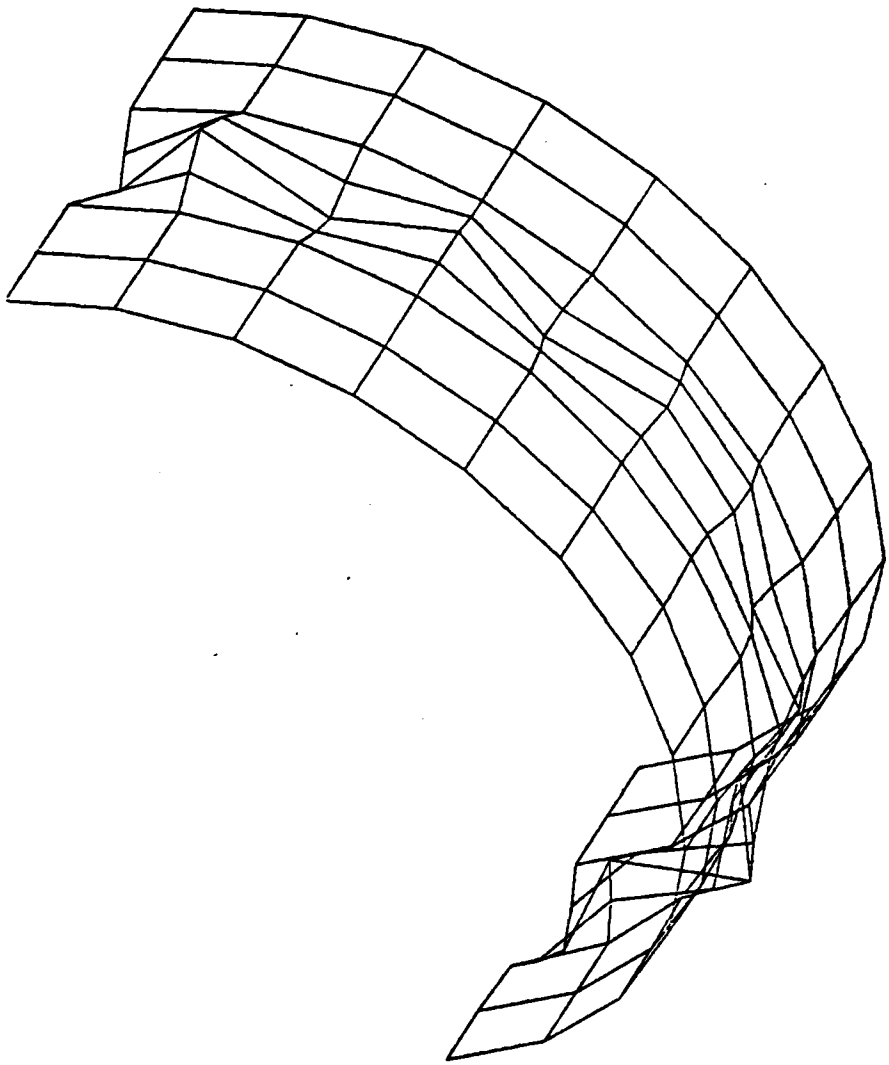

FIGURE 27. STIFFENED CYLINDRICAL SHELL. SAME AS FIGURE 26. (u, v, w) COMBINED DEFORMATION MODE. $\Delta p_{cr} = 316.04$ LB/IN^2

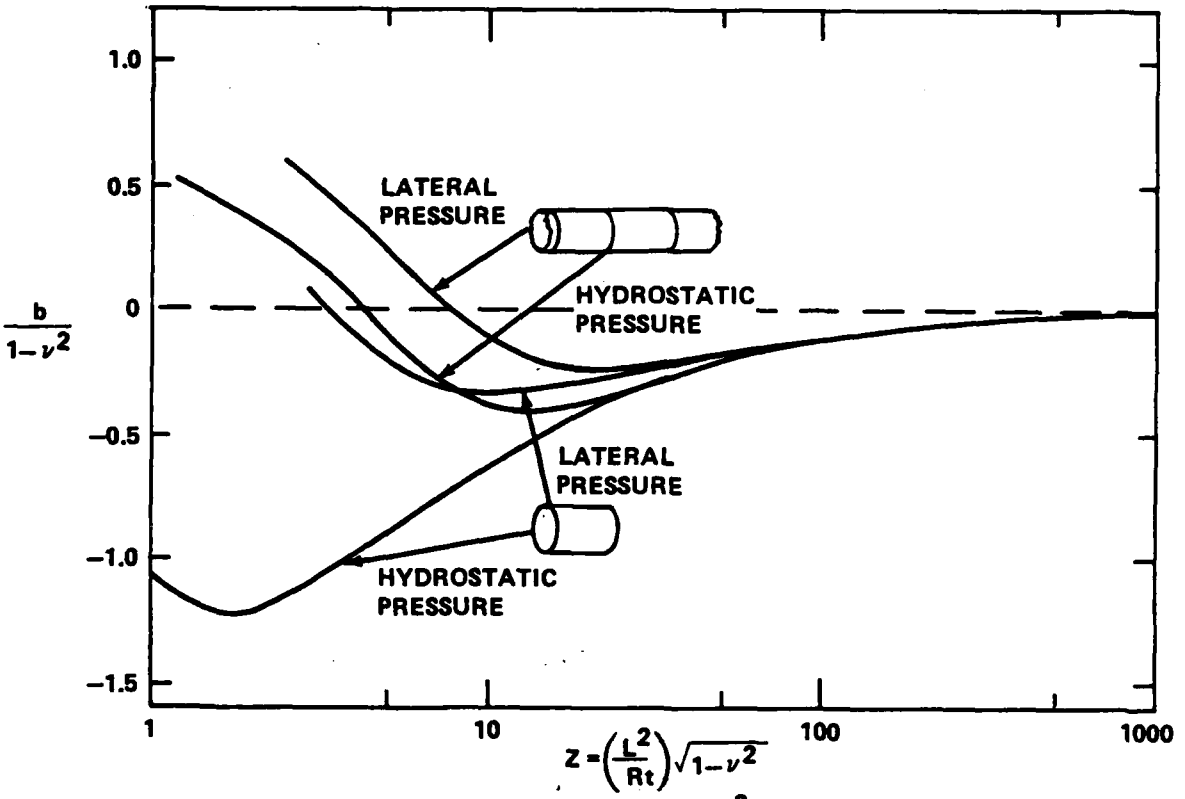

FIGURE 28. BATDORF PARAMETER Z VERSUS b/(1− ν^2) FOR 2 TYPES OF CYLINDERS AND 2 TYPES OF LOADINGS (FIGURE REPRODUCED FROM REFERENCE (10))

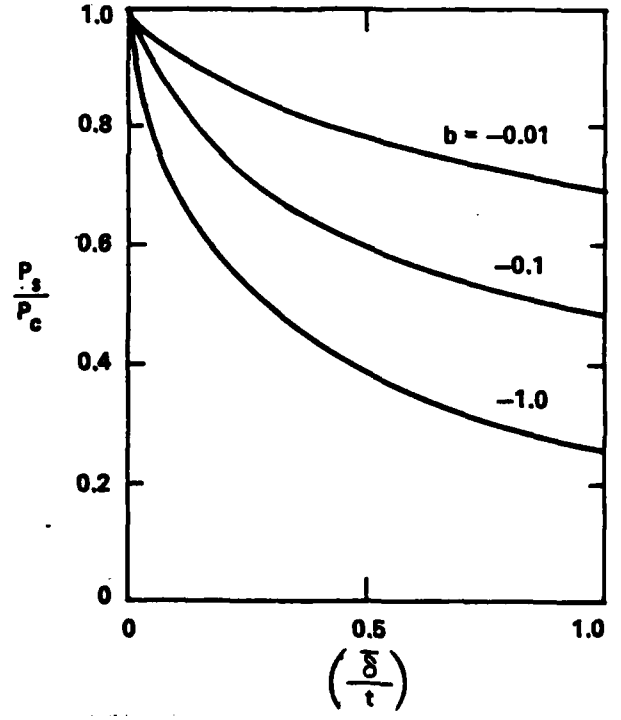

FIGURE 29. (Ps/Pc) VERSUS (δ/t) FOR VARIOUS VALUES OF b (FIGURE REPRODUCED FROM REFERENCE (10))

imperfection. This compares with 283.88 Lb/in^2 of Table 7, and confirms the expected result that imperfections lower the critical pressure. (Furthermore, it suggests that 263.38 Lb/in^2, as obtained by the full model (Table 1, Case 1), is an artificial characteristic root.)

6. GENERAL COMMENTS

We note that the presence of the hole (Cases 2 and 3 of Table 6) appears to remove the lowest eigenvalue obtained in the model without a hole (see Table 1, Case 1), which appears to be a spurious result. The present results (272.94 Lb/in^2, 266.26 Lb/in^2) compare well with the second one of Case 1 Table 1 (Δp = 293.74 Lb/in^2). Similarly, Cases 2 and 3 (Table 6) compare with Case 2, Table 1, in which the imperfection (Case 1, Table 7) again seems to have caused the lowest eigenvalue to be missed.

TABLE 7.

EFFECT OF IMPERFECTIONS ON CRITICAL PRESSURE

Case	Type of Model	Element Type	Mesh in Middle Bays	Δp_{cr} (lb/in^2)
1	Full Cylinder as in Case 1, Table 1, with imperfections (given as Case 10 on Table 1)	410	5 x 25	283.88
2	Half Cylinder as in Case 2, Table 1, with Imperfections (θ = o)	410	5 x 13	316.04
3	As Case 2 except that angular location of maximum imperfection at $\theta = 10^o$	410	5 x 13	316.04

CHAPTER 5

CONCLUSIONS AND SUGGESTIONS FOR FURTHER WORK

In this report only the bifurcation option (linear stress state) of STAGS was studied by analyzing a portion of a ring stiffened cylinder subject to hydrostatic loading. The critical pressure obtained was about 280 Lb/in^2.

The following conclusions may be drawn from all these studies:

(a) Employ the analytic formulae to obtain an approximate value for the critical load. Start at a higher baseload. Analyze the entire cylinder peripherally, but half axially. If such a model is too big, then use half the model peripherally and employ symmetry conditions there. Treat the resulting answers as approximate.

(b) Do not employ a very fine mesh, as it may tend to bypass the critical pressure.

(c) Element 410 is as good as Element 411 for buckling.

(d) A hole appears to degrade the critical load slightly. The actual amount depends on the hole size.

(e) If imperfections are used, it is preferable to use the full cylinder model.

In the use of circular cylinders subject to hydrostatic loading, both the structure and the load are symmetrical and the prebuckling behavior is nonlinear. Collapse may occur in an axisymmetric way at a limit point or in an asymmetric mode if bifurcation occurs. These modes can be analyzed by carrying

out a nonlinear stepwise analysis under increasing load (with or without imperfections). Another possibility is to carry out a dynamic analysis of the same structure and loading over a time much larger than the natural period of excitation of the structure, and thereby obtain a load deflection path. For the last one, estimates of the natural period of excitation are necessary.

BIBLIOGRAPHY

Almroth, B. O., and Brogan, F. A., "Computational Efficiency of Shell Elements," in AMD-Vol. 48, Nonlinear Finite Element Analysis of Plates and Shells, The American Society of Mechanical Engineers, Washington, D.C., 15-20 Nov 1981.

Almroth, B. O., Brogan, F. A., and Stanley, G. M., Structural Analysis of General Shells, Vol. II, User Instruction for STAGSC, LMSC-D633873, Apr 1979.

Brendel, B., and Ramm, E., "Linear and Nonlinear Stability Analysis of Cylindrical Shells," Journal of Computers and Structures, Vol. 12, 1980, pp. 549-558.

Brogan, F., and Almroth, B. O., "Buckling of Cylinders with Cutouts," AIAA Journal, Vol. 8, No. 2, Feb 1970, pp. 236-240.

Brogan, F. A., and Almroth, B. O., "Practical Methods for Elastic Collapse Analysis for Shell Structures," AIAA Journal, Vol. 9, No. 12, Dec 1971, pp. 2321-2326.

Budiansky, B. E., and Amazigo, J. C., "Initial Post-buckling Behavior of Cylindrical Shells Under External Pressure," Journal of Mathematics and Physics, Vol. 47, 1968, pp. 223-235.

Bushnell, D., "Buckling of Shells-Pitfalls for Designers," AIAA Journal, Vol. 19, No. 9, Sep 1981, pp. 1183-1226.

Fluegge, W., "Die Stabilitaet der Kreiszylinderschale," Ingenieur Archiv, Vol. 3, pp. 463-506, 1932.

Moussouros, M., Comparisons of Static Collapse Predictions of a Ring Stiffened Cylindrical Shell Subject to Hydrostatic Pressure, NSWC TR 81-325, 3 Mar 1982.

Renzi, J. R., Optimization of Orthotropic, Non-Linear, Ring-Stiffened Cylindrical Shells Under External Hydrostatic Pressure as Applied to MMC Materials, NSWC TR 79-305, 30 Sep 1979.

Thomas, K., and Sobel, L. A., Evaluation of the STAGSC - 1 Shell Analysis Computer Program, Westinghouse Electric Corporation, Report No. Ward-10881, Aug 1981.

Timoshenko, S. P., and Gere, J. M., Theory of Elastic Stability, McGraw-Hill Book Co., Second Edition, pp. 457-519, 1961.

Windenberg, D. F., and Trilling, C., "Collapse by Instability of Thin Cylindrical Shells Under External Pressure," Transaction of ASME, Journal of Applied Mechanics, Vol. 56, No. 11, pp. 819-825, Nov 1934.

TERMS

U_r	Translation radially outwards
U_x	Translation in longitudinal direction (X-axis)
U_θ	Translation along the tangential axis
U_{rr}	Rotation about the radial axis
U_{xx}	Rotation about the longitudinal axis (X-axis)
$U_{\theta\theta}$	Rotation about the tangential axis

APPENDIX A

SELECTED COMPUTER OUTPUT

TABLE A-1. MODE 1 TRANSLATIONS (u,v,w) FOR DEAD LOAD PRESSURE, CASE 1, TABLE 1. AT x = 1.5s, Δp_{cr} = 263.38 Lb/in^2

UNIT 2 (SHELL) DISPLACEMENTS MODE 1

ROW	COL	X	Y	U	V	W
3	1	15.000	0.000	-.91814E-08	-.57695E-04	-.10120E-04
3	2	15.000	15.000	-.24258E-05	.15225E-03	-.40478E-04
3	3	15.000	30.000	-.13423E-05	-.33225E-04	-.80719E-04
3	4	15.000	45.000	.75355E-06	.18017E-03	-.10395E-04
3	5	15.000	60.000	.26060E-05	-.20186E-04	.74467E-05
3	6	15.000	75.000	.25416E-05	.17200E-03	.55465E-04
3	7	15.000	90.000	-.96169E-06	-.44581E-04	.67227E-04
3	8	15.000	105.000	-.42559E-05	.14502E-03	.20268E-04
3	9	15.000	120.000	-.35026E-05	-.61915E-04	.27204E-04
3	10	15.000	135.000	.23138E-06	.14103E-03	-.36645E-04
3	11	15.000	150.000	.38293E-05	-.54541E-04	-.14519E-04
3	12	15.000	165.000	.40446E-05	.15216E-03	-.23542E-04
3	13	15.000	180.000	.28504E-07	-.46209E-04	-.86623E-05
3	14	15.000	195.000	-.40498E-05	.15355E-03	.29187E-04
3	15	15.000	210.000	-.37929E-05	-.52337E-04	.55666E-05
3	16	15.000	225.000	-.26614E-06	.14389E-03	.36512E-04
3	17	15.000	240.000	.34903E-05	-.59623E-04	-.18569E-04
3	18	15.000	255.000	.42049E-05	.14652E-03	-.26049E-04
3	19	15.000	270.000	.94081E-06	-.44594E-04	-.48478E-04
3	20	15.000	285.000	-.25429E-05	.17044E-03	-.61414E-04
3	21	15.000	300.000	-.26142E-05	-.22681E-04	.25802E-05
3	22	15.000	315.000	-.71815E-06	.17696E-03	.10167E-04
3	23	15.000	330.000	.13271E-05	-.35745E-04	.71052E-04
3	24	15.000	345.000	.24820E-05	.15062E-03	.46916E-04
3	25	15.000	360.000	-.91814E-08	-.57695E-04	-.10120E-04

TABLE A-2. MODE 1 TRANSLATIONS (u,v,w) FOR LIVE PRESSURE AS CASE 1, TABLE 1. AT $x = 1.5s$, $\Delta p_{cr} = 280.14$ Lb/in^2

UNIT 2 (SHELL) DISPLACEMENTS MODE 1

ROW	COL	X	Y	U	V	W
3	1	15.000	0.000	-.21769E-07	-.26531E-03	-.98991E-05
3	2	15.000	15.000	-.21822E-05	.34209E-03	-.34139E-04
3	3	15.000	30.000	-.11660E-05	-.24627E-03	-.53640E-04
3	4	15.000	45.000	.62980E-06	.36500E-03	-.30488E-04
3	5	15.000	60.000	.23785E-05	-.23439E-03	.26517E-04
3	6	15.000	75.000	.21231E-05	.35938E-03	.20179E-04
3	7	15.000	90.000	-.79048E-06	-.25406E-03	.79375E-04
3	8	15.000	105.000	-.37456E-05	.33610E-03	.34362E-05
3	9	15.000	120.000	-.29339E-05	-.26972E-03	.38239E-04
3	10	15.000	135.000	.17832E-06	.33258E-03	-.46568E-04
3	11	15.000	150.000	.33192E-05	-.26243E-03	-.50748E-05
3	12	15.000	165.000	.34344E-05	.34336E-03	-.31281E-04
3	13	15.000	180.000	.17228E-07	-.25520E-03	.63295E-05
3	14	15.000	195.000	-.34319E-05	.34272E-03	.24271E-04
3	15	15.000	210.000	-.32644E-05	-.26308E-03	.12018E-04
3	16	15.000	225.000	-.16059E-06	.33216E-03	.36587E-04
3	17	15.000	240.000	.29412E-05	-.26966E-03	-.32253E-04
3	18	15.000	255.000	.36988E-05	.33586E-03	-.67212E-05
3	19	15.000	270.000	.77042E-06	-.25446E-03	-.73489E-04
3	20	15.000	285.000	-.20808E-05	.35856E-03	-.22552E-04
3	21	15.000	300.000	-.23140E-05	-.23467E-03	-.29975E-04
3	22	15.000	315.000	-.56260E-06	.36484E-03	.34564E-04
3	23	15.000	330.000	.11589E-05	-.24584E-03	.42454E-04
3	24	15.000	345.000	.21938E-05	.34216E-03	.52219E-04
3	25	15.000	360.000	-.21769E-07	-.26531E-03	-.98991E-05

TABLE A-3. MODE 1 TRANSLATIONS (u,v,w) FOR DEAD LOAD PRESSURE ON PANEL OF ARC $\theta^o = 120^o$ IN THE MIDDLE OF BAY AS PER TABLE 3, FIGURE 17. $\Delta p_{cr} = 259.0$ Lb/in^2

UNIT 1 (SHELL) DISPLACEMENTS MODE 1

ROW	COL	X	Y	U	V	W
2	1	5.000	30.000	.56503E-03	0.	-.98337E+00
2	2	5.000	40.000	.54570E-03	.16830E+00	-.94989E+00
2	3	5.000	50.000	.48925E-03	.32513E+00	-.85167E+00
2	4	5.000	60.000	.39945E-03	.45981E+00	-.69539E+00
2	5	5.000	70.000	.28199E-03	.56315E+00	-.49172E+00
2	6	5.000	80.000	.14514E-03	.62811E+00	-.25453E+00
2	7	5.000	90.000	-.15796E-05	.65027E+00	.13127E-04
2	8	5.000	100.000	-.14821E-03	.62811E+00	.25454E+00
2	9	5.000	110.000	-.28455E-03	.56315E+00	.49171E+00
2	10	5.000	120.000	-.40143E-03	.45981E+00	.69537E+00
2	11	5.000	130.000	-.49107E-03	.32513E+00	.85164E+00
2	12	5.000	140.000	-.54731E-03	.16830E+00	.94989E+00
2	13	5.000	150.000	-.56641E-03	0.	.98341E+00

DISTRIBUTION

	Copies
Chief of Naval Material	
Attn: CAPT G. Jarrett (ASW-14)	1
Dr. A. J. Faulstich (MAT 07)	1
Navy Department	
Washington, D.C. 20360	
Commander	
Naval Sea Systems Command	
Attn: SEA-03B	1
SEA 63R (F. Romano)	1
SEA-63R32 (Murphy)	1
SEA-9G32	1
SEA-32R (C. Pohler)	1
SEA-3221 (H. Ward)	1
PMS-402	1
PMS-406	1
PMS-407	1
Department of the Navy	
Washington, D.C. 20362	
Commander	
David W. Taylor Naval Ship Research & Development Center	
Attn: Code 17 (Dr. W. Murray)	1
Code 175 (J. Sykes)	1
Code 175.2 (B. Whang)	1
Code 175.2 (T. Giacofci)	1
Code 175.2 (T. Gilbert)	1
Code 175.3 (W. Conley)	1
Code 175.3 (P. Manny)	1
Code 184.4 (M. Hurwitz)	1
Code 172 (M. Krenzke)	1
Code 1620.3 (R. Jones)	1
Bethesda, Maryland 20084	
David W. Taylor Naval Ship Research and Development Center	
Attn: Code 177 (R. Fuss)	1
Code 177.1 (V. Bloodgood)	1
Code 177.1 (M. Riley)	1
Code 177.1(R. Higginbotham)	1
Underwater Explosion Research Division	
Portsmouth, Virginia 23709	

	Copies
Commander	
Naval Weapons Center	
Attn: Code 533 (Technical Library)	1
China Lake, California 93555	
Commander	
Naval Ocean Systems Center	
Attn: Technical Library	1
San Diego, California 92152	
Commanding Officer	
Naval Underwater Systems Center	
Attn: (D. J. Lepore)	1
Newport, Rhode Island 02840	
Office of Naval Research	
Attn: Code 474 (D. N. Basdekas)	1
800 North Quincy Street	
Arlington, Virginia 22217	
Defense Nuclear Agency	
Attn: SPSS (LT D. Sobota)	1
Washington, D.C. 20305	
Defense Technical Information Center	
Cameron Station	
Alexandria, Virginia 22314	12
Library of Congress	
Attn: Gift and Exchange Division	4
Washington, D.C. 20540	
Internal Distribution:	
R10	1
R102	2
R14	20
R14 (M. Moussouros)	1
E431	9
E432	3
E35	1

END

FILMED

9-83

DTIC